WAVE STRUCTURE SIMILARITY OF THE HLLC AND ROE RIEMANN SOLVERS: APPLICATION TO LOW MACH NUMBER PRECONDITIONING*

MARICA PELANTI†

Abstract. The approximate Riemann solver of Roe and the solver of Harten–Lax–van Leer (HLL) and its variants, such as the HLLC solver, are widely used as building blocks of finite volume Godunov-type methods for the solution of the Euler equations of gas dynamics and related hyperbolic flow models. The HLLC solver has gained increasing popularity over the last two decades since it possesses some of the good properties of the Roe solver and in addition it satisfies important entropy and positivity conditions with no need of special fixes. In this work we rewrite the classical HLLC Riemann solver in a novel form that highlights the formal mathematical similarity of its wave structure with the one of the Roe solver. This similarity might be useful to extend to the HLLC method some numerical techniques devised specifically for the Roe's method. As an example of application we illustrate the design of a Turkel-type low Mach number preconditioning technique for the HLLC scheme by exploiting methodologies proposed in the literature for the Roe's scheme.

Key words. Approximate Riemann solvers, Roe solver, HLLC solver, finite volume schemes, Euler equations, low Mach number preconditioning.

AMS subject classifications. 65M08,76N99

1. Introduction.

Finite volume Godunov-type schemes [14] based of Riemann solvers are powerful methods to compute solutions to hyperbolic systems of equations, which arise in numerous areas of science. In the context of Computational Fluid Dynamics, some of the most popular approximate Riemann solvers are the celebrated solver of Roe [38] (1981) and the solver of Harten–Lax–van Leer (HLL) [21] (1983) and its variants, such as the HLLEM and the HLLC solvers. We refer the reader in particular to the monographs [43, 25] for a comprehensive presentation of Riemann solvers and Godunov-type methods. The HLLC solver (HLL with Contact restoration) introduced by Toro, Spruce and Speares [44] (1994) for the Euler equations of gas dynamics has especially gained increasing popularity over the last two decades. This solver was conceived to improve the original HLL solver by enriching its approximate wave structure consisting of two waves with an additional intermediate wave representing the contact wave of the Euler equations. While both the Roe solver and the HLLC solver have the advantage of embedding the description of the contact wave, the HLLC solver possesses very important additional properties: it is entropy-satisfying and positivity-preserving, when suitable definitions of the wave speeds are used. In contrast, it is well known that the Roe solver needs an entropy fix to converge to the physically relevant entropic solution and it also requires special fixes to ensure positivity of computed values of densities and energies (e.g. [34]), which might be difficult to devise for some complex flow models. Furthermore, the HLLC solver does not need the definition of a special average state to fulfill conservation as the Roe solver. Thanks to all these desirable properties the HLLC solver has been widely adopted in recent years for the solution of numerous flow models related to the basic Euler equations, in particular for applications to multifluid and multiphase compressible flow models [42, 40, 35, 13, 39, 33]. Let us also recall that the HLLC solver is equivalent to the Suliciu's relaxation Riemann solver [6], for which Bouchut has rigorously demonstrated positivity and entropy conditions.

In the present work we rewrite the classical HLLC Riemann solver in a novel form that

*Submitted to the editors November 1, 2017.

Funding: This work was partially funded by the French Government Directorate for Armament (DGA) under Grant N. 2012.60.0011.00.470.75.01.

†Institute of Mechanical Sciences and Industrial Applications, UMR 9219 ENSTA ParisTech-EDF-CNRS-CEA, 828 Boulevard des Maréchaux, 91762 Palaiseau, France (marica.pelanti@ensta-paristech.fr).

highlights the formal mathematical similarity of its wave structure with the one of the Roe solver. In particular, we show that the acoustic waves of the HLLC solver, similar to the Roe solver, are collinear to vectors corresponding to the eigenvectors of the Euler equations associated to the acoustic fields evaluated in a special state that is a function of the left and right Riemann data. The strengths of these waves have also expressions in terms of jumps in pressure and normal velocity analogous to those of the Roe solver. Our novel reformulation of the HLLC solver is based on very simple algebraic manipulations, yet it seems that this form has not been shown in the existing literature. The revealed mathematical similarity of the wave structure of the two solvers might be useful to extend to the HLLC method some numerical techniques devised specifically for the Roe's method. In fact, certain algorithms exploit the average eigenstructure of the Roe matrix, and they cannot be adapted to the HLLC solver in a straightforward manner. As an example of application we consider in this work low Mach number preconditioning techniques aimed to cure the well known difficulty of severe loss of accuracy of upwind schemes for compressible flows at low Mach number regimes. These preconditioning strategies have been developed and studied considerably for the Roe's scheme [19, 41, 10, 27, 29, 28, 36, 16, 18], but extensions to the HLLC scheme are scarce [31, 23] and often lack rigorous analyses. Here in particular we will follow closely the work of Guillard and Viozat [19] and extend the study and strategies therein for the Roe's method to the HLLC method. Thanks to the revealed formal analogy of the acoustic waves of the two considered solvers first we can give an analytical explanation of the loss of accuracy of the HLLC method at low Mach number, and then we are able to propose a Turkel-type preconditioning technique to overcome this difficulty that mimics the preconditioned Roe-Turkel method of Guillard–Viozat [19]. An extension of the proposed HLLC-Turkel method to a two-phase compressible flow model has been already presented by the author in [33]. Indeed, the work in the present article originated from an investigation of low Mach number corrections applicable to Roe-type and HLLC-type schemes that the author had developed for a six-equation two-phase flow model introduced in previous work [35]. Although we have partially anticipated in [33] the study on the similarity of the Roe and the HLLC solvers, here we provide a more detailed and extensive analysis, presenting also a unified formulation of the semi-discrete equations of the two schemes (Appendix B).

This article is organized as follows. We first recall the Euler equations of gas dynamics in section 2 and the Roe and HLLC Riemann solvers in subsection 3.1 and subsection 3.2, respectively. The new formulation of the HLLC solver is presented in subsection 3.3. We illustrate in section 4 an application to low Mach number preconditioning, introducing in subsection 4.4 a new HLLC-Turkel scheme. Some conclusions are written in section 5.

2. The Euler equations of gas dynamics. The classical Euler equations governing an inviscid compressible flow can be written in two spatial dimensions in the following conservative form:

$$\partial_t q + \partial_x f(q) + \partial_y g(q) = 0, \tag{1a}$$

where

$$q = \begin{pmatrix} \rho \\ \rho u \\ \rho v \\ E \end{pmatrix}, \quad f(q) = \begin{pmatrix} \rho u \\ \rho u^2 + p \\ \rho uv \\ u(E+p) \end{pmatrix}, \quad g(q) = \begin{pmatrix} \rho v \\ \rho vu \\ \rho v^2 + p \\ v(E+p) \end{pmatrix}. \tag{1b}$$

Here ρ is the fluid density, u and v are the flow velocity components in the x and y direction, respectively, p is the pressure, and E is the total energy per unit volume, $E = \mathcal{E} + \rho\frac{|\vec{u}|^2}{2}$,

where $\mathcal{E}$ denotes the internal energy per unit volume, and $\vec{u} = (u, v)$. The system is closed through the specification of a pressure law $p = p(\mathcal{E}, \rho)$. The Euler system is hyperbolic and the eigenvalues associated to the direction $\vec{n} = (n_x, n_y)$, $|\vec{n}| = 1$, are $\lambda_{1,4} = \vec{u} \cdot \vec{n} \mp c$ and $\lambda_l = \vec{u} \cdot \vec{n}$ for $l = 2, 3$ (eigenvalue of algebraic multiplicity 2). The speed of sound is $c = \sqrt{\kappa h + \chi}$, where $\kappa = \frac{\partial p(\mathcal{E},\rho)}{\partial \mathcal{E}}$, $\chi = \frac{\partial p(\mathcal{E},\rho)}{\partial \rho}$, and h denotes the specific enthalpy, $h = \frac{\mathcal{E}+p}{\rho}$. In this wok a stiffened gas equation of state will be assumed, which allows us to use a standard Roe linearization: $p(\mathcal{E}, \rho) = (\gamma - 1)\mathcal{E} - (\gamma - 1)\eta\rho - \gamma\varpi$, where γ, η, ϖ are material-dependent constant parameters. Hence here $\kappa = (\gamma - 1)$ and $\chi = -(\gamma - 1)\eta$.

3. Finite Volume Schemes based on Riemann solvers. Finite volume schemes based on Riemann solvers (Godunov-type schemes) are widely used to approximate solutions to the Euler equations. Here we recall this class of schemes by adopting the wave propagation formulation by LeVeque [24, 25]. Let us consider a general hyperbolic system of the form

$$\partial_t q + A(q)\partial_x q + B(q)\partial_y q = 0. \tag{2}$$

Clearly the Euler equations (1) can be written in this quasi-linear form with $A(q) = f'(q)$ and $B(q) = g'(q)$, $A, B \in \mathbb{R}^{4\times4}$. We assume here a spatial discretization on a Cartesian grid with cells of uniform size Δx and Δy in the x and y directions, respectively. We denote by $q_{i,j}$ the approximate solution of the system at the cell (i, j), $i, j \in \mathbb{Z}$. The two-dimensional first-order wave propagation algorithm [24, 25] has the semi-discrete form

$$\frac{dq_{i,j}}{dt} + \frac{1}{\Delta x}\left(\mathcal{A}^+\Delta Q_{i-1/2,j} + \mathcal{A}^-\Delta Q_{i+1/2,j}\right) + \frac{1}{\Delta y}\left(\mathcal{B}^+\Delta Q_{i,j-1/2} + \mathcal{B}^-\Delta Q_{i,j+1/2}\right) = 0. \tag{3}$$

Here $\mathcal{A}^\pm\Delta Q$ and $\mathcal{B}^\pm\Delta Q$ are the so-called fluctuations arising from the solution of local plane-wave Riemann problems in the x and y directions, respectively [24]. More precisely, the left-going fluctuations $\mathcal{A}^-\Delta Q_{i+1/2,j}$ and the right-going fluctuations $\mathcal{A}^+\Delta Q_{i+1/2,j}$ are computed by solving local Riemann problems for the system $\partial_t q + A(q)\partial_x q = 0$ at cell interfaces $x_{i+1/2,j}$ for each pair of data $q_{i,j}$, $q_{i+1,j}$ corresponding to adjacent cells (i, j) and $(i+1, j)$. In a similar way, the fluctuations $\mathcal{B}^\mp\Delta Q_{i,j+1/2}$ are computed by solving Riemann problems for $\partial_t q + B(q)\partial_y q = 0$ at cell interfaces $x_{i,j+1/2}$ between adjacent cells (i, j) and $(i, j + 1)$. A Riemann solver (cf. [43, 25]) must be provided to compute solutions to local Riemann problems. Let us now consider with no loss of generality the approximation of a two-dimensional plane-wave Riemann problem in the x direction for the Euler equations, namely a Riemann problem for the system $\partial_t q + \partial_x f(q) = 0$, with initial left and right data q_ℓ and q_r. The exact solution of this problem consists of at most four constant states separated by a 1-wave (shock or rarefaction), a contact discontinuity corresponding to the eigenvalue $\lambda_2 = \lambda_3 = u$, and a 4-wave (shock or rarefaction), when a convex equation of state is assumed. The solution structure defined by an approximate Riemann solver can be expressed in general by a set of $\mathscr{M}$ waves $\mathcal{W}^l$ and corresponding speeds s^l, $\mathscr{M} \geq 2$ (e.g. $\mathscr{M} = 2$ for the HLL solver, $\mathscr{M} = 4$ for Roe solver). The sum of the waves $\mathcal{W}^l$ must be equal to the initial jump in the vector q of the system's variables:

$$\Delta q \equiv q_r - q_\ell = \sum_{l=1}^{\mathscr{M}} \mathcal{W}^l. \tag{4}$$

Moreover, waves and speeds must satisfy the following conservation condition:

$$\Delta f(q) \equiv f(q_r) - f(q_\ell) = \sum_{l=1}^{\mathscr{M}} s^l\mathcal{W}^l. \tag{5}$$

Once the Riemann solution structure $\{\mathcal{W}^l_{i+1/2,j}, s^l_{i+1/2,j}\}_{l=1,\dots,\mathscr{M}}$ associated to each cell pair $\{(i,j),(i+1,j)\}$ is defined through a Riemann solver, the fluctuations $\mathcal{A}^{\mp}\Delta Q_{i+1/2,j}$ in (3) are computed as

$$\mathcal{A}^{\mp}\Delta Q_{i+1/2,j} = \sum_{l=1}^{\mathscr{M}} (s^l_{i+1/2,j})^{\mp} \mathcal{W}^l_{i+1/2,j}\,, \tag{6}$$

where $s^+ = \max(s,0)$ and $s^- = \min(s,0)$. The first-order scheme (3) can be extended to second-order accuracy by adding suitable correction terms, which can be expressed again in terms of waves and speeds. Here we are mainly interested in studying the performance of simple first-order methods, however for one test case (Section 4.6.2) we will also present results obtained with second-order corrections of the form [25]

$$\tilde{F}_{i+1/2,j} = \frac{1}{2}\sum_{l=1}^{\mathscr{M}} |s^l_{i+1/2,j}| \left(1 - \frac{\Delta t}{\Delta x} s^l_{i+1/2,j}\right) \widetilde{\mathcal{W}}^l_{i+1/2,j}\,. \tag{7}$$

Here Δt is the time step and $\widetilde{\mathcal{W}}^l_{i+1/2,j}$ is a limited version of the wave $\mathcal{W}^l_{i+1/2,j}$, $\widetilde{\mathcal{W}}^l_{i+1/2,j} = \phi(\theta^l_{i+1/2,j})\mathcal{W}^l_{i+1/2,j}$, where ϕ is a limiter function, and $\theta^l_{i+1/2,j}$ a measure of the smoothness of the solution, obtained by comparing $\mathcal{W}^l_{i+1/2,j}$ with $\mathcal{W}^l_{I+1/2,j}$, $I = i-1$ if $s^l_{i+1/2,j} > 0$, and $I = i+1$ if $s^l_{i+1/2,j} < 0$. Let us remark that in order to achieve formal second-order accuracy contributions of transverse fluctuations [24] need also to be included in the two-dimensional algorithm (3). However transverse corrections are not considered in the present study. Let us also note that the methods described here can be generalized in a straightforward manner to logically rectangular quadrilateral grids (curvilinear grids). We refer the reader to [24, 25] for an exhaustive presentation of these wave propagation algorithms. Omitting for simplicity from now on j indexes associated to the y direction, let us also recall the relation between the fluctuations $\mathcal{A}^{\mp}\Delta Q_{i+1/2}$ and interfacial numerical fluxes $F_{i+1/2} = \varphi(q_i, q_{i+1})$ used in more classical formulations of Godunov-type Finite Volume schemes:

$$F_{i+1/2} = f(q_i) + \mathcal{A}^-\Delta Q_{i+1/2} = f(q_{i+1}) - \mathcal{A}^+\Delta Q_{i+1/2}. \tag{8}$$

The numerical flux $F_{i+1/2}$ can be usually expressed as the sum of a central term and a numerical dissipation term $\mathcal{V}\Delta Q_{i+1/2}$:

$$F_{i+1/2} = \frac{1}{2}(f(q_i) + f(q_{i+1})) - \frac{1}{2}\mathcal{V}\Delta Q_{i+1/2}\,. \tag{9}$$

For many schemes one can write $\mathcal{V}\Delta Q_{i+1/2} = \Theta_{i+1/2}(q_{i+1} - q_i)$, where $\Theta_{i+1/2} = \vartheta(q_i, q_{i+1})$ is the numerical dissipation matrix (viscosity matrix). The fluctuations (6) can be then expressed equivalently in terms of flux differences and numerical dissipation terms as

$$\mathcal{A}^{\pm}\Delta Q_{i+1/2} = \frac{1}{2}\Delta f_{i+1/2} \pm \frac{1}{2}\mathcal{V}\Delta Q_{i+1/2}\,, \tag{10}$$

where

$$\mathcal{V}\Delta Q_{i+1/2} = \sum_{l=1}^{\mathscr{M}} |s^l_{i+1/2}| \mathcal{W}^l_{i+1/2}\,, \tag{11}$$

and $\Delta f_{i+1/2} \equiv f(q_{i+1}) - f(q_i)$ is defined in terms of waves $\mathcal{W}^l_{i+1/2}$ and speeds $s^l_{i+1/2}$ through the conservation condition (5).

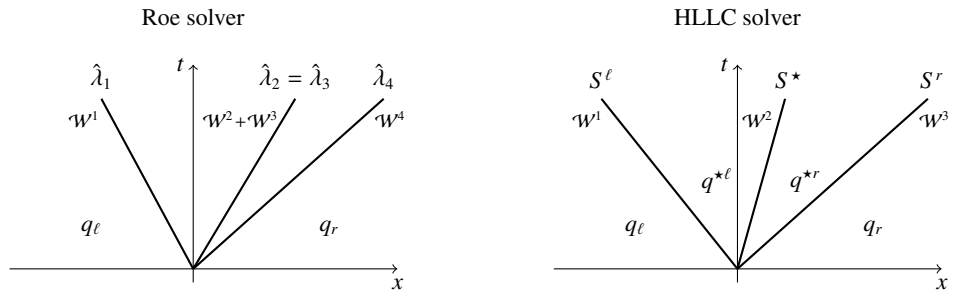

FIG. 1. *Solution structure of the Roe solver (left) and of the HLLC solver (right) approximating the solution of a plane-wave Riemann problem in the x direction for the two-dimensional Euler equations.*

3.1. Roe approximate Riemann solver. The idea of the celebrated approximate Riemann solver of Roe [38] is to define an approximate solution to a Riemann problem for the Euler equations $\partial_t q + \partial_x f(q) = 0$, with q and $f(q)$ as in (1), by the exact solution of a Riemann problem for a linearized system $\partial_t q + \hat{A}(q_\ell, q_r)\partial_x q = 0$. The constant coefficient matrix $\hat{A} = \hat{A}(q_\ell, q_r)$ (Roe matrix) is defined locally by evaluating the Jacobian $A(q) = f'(q)$ of the original system in a suitable average state $\hat{q} = \hat{q}(q_\ell, q_r)$. This average state must be chosen so that the Roe matrix $\hat{A}$ satisfies the conservation consistency relations (5), which can be equivalently written as $f(q_r) - f(q_\ell) = \hat{A}(q_r - q_\ell)$. The Riemann solution structure of the Roe solver consists of $\mathscr{M} = 4$ waves and speeds that correspond to the eigenstructure of the Roe matrix (see Figure 1). Denoting with $\hat{r}_l$ and $\hat{\lambda}_l$ the right eigenvectors and eigenvalues of $\hat{A}$, respectively, we have

$$\mathcal{W}^l = \hat{\zeta}_l \hat{r}_l \qquad \text{and} \qquad s^l = \hat{\lambda}_l\,, \quad l = 1, \cdots, 4, \tag{12}$$

where $\hat{\zeta}_l$ are the coefficients of the projection of the jump $\Delta q \equiv q_r - q_\ell$ onto the basis of the Roe eigenvectors, $q_r - q_\ell = \sum_{l=1}^{4} \hat{\zeta}_l \hat{r}_l$. The definition of the Roe eigenstructure is reported in Appendix A. Considering now $q_\ell = q_i$, $q_r = q_{i+1}$, and denoting $\hat{A}_{i+1/2} = \hat{A}(q_i, q_{i+1})$, we can write the numerical dissipation term (11) of the Roe's scheme as

$$\mathcal{V}\Delta Q_{i+1/2} = \sum_{l=1}^{4} (|\hat{\lambda}_l|\hat{\zeta}_l \hat{r}_l)_{i+1/2} = \hat{R}_{i+1/2}|\hat{\Lambda}_{i+1/2}|\hat{R}^{-1}_{i+1/2}(q_{i+1} - q_i) = |\hat{A}_{i+1/2}|(q_{i+1} - q_i), \tag{13}$$

where $\hat{R} = [\hat{r}_1 \dots \hat{r}_4]$ and $\hat{\Lambda} = \mathrm{diag}(\hat{\lambda}_1, \dots, \hat{\lambda}_4)$. The viscosity matrix is $\Theta = |\hat{A}|$.

3.2. HLLC approximate Riemann solver. The Riemann solution structure of the HLLC solver of Toro *et al.* [44] consists of three waves $\mathcal{W}^l$, $l = 1, 2, 3$ ($\mathscr{M} = 3$), moving at speeds

$$s^1 = S^\ell\,, \quad s^2 = S^\star\,, \quad \text{and} \quad s^3 = S^r, \tag{14}$$

which separate four constant states q_ℓ, $q^{\star\ell}$, $q^{\star r}$ and q_r (see Figure 1). In the following we will indicate with $(\cdot)_\ell$ and $(\cdot)_r$ quantities corresponding to the states q_ℓ and q_r, respectively. Moreover, we will indicate with $(\cdot)^{\star\ell}$ and $(\cdot)^{\star r}$ quantities corresponding to the states $q^{\star\ell}$ and $q^{\star r}$ adjacent, respectively on the left and on the right, to the middle wave propagating at speed $S^\star$. With this notation, the waves of the HLLC solver are

$$\mathcal{W}^1 = q^{\star\ell} - q_\ell, \quad \mathcal{W}^2 = q^{\star r} - q^{\star\ell}, \quad \text{and} \quad \mathcal{W}^3 = q_r - q^{\star r}. \tag{15}$$

Then, the following conservation conditions are imposed (sufficient to satisfy (5)):

$$f(q^{\star\ell}) - f(q_\ell) = S^\ell(q^{\star\ell} - q_\ell), \tag{16a}$$

$$f(q^{\star r}) - f(q^{\star\ell}) = S^\star(q^{\star r} - q^{\star\ell}), \tag{16b}$$

$$f(q_r) - f(q^{\star r}) = S^r(q_r - q^{\star r}). \tag{16c}$$

Additionally, invariance of the pressure p and of the normal velocity u is assumed across the 2-wave, in analogy with the exact Riemann solution. Then the speed $S^\star$ is determined as [43]

$$S^\star = \frac{\Delta p + \rho_\ell u_\ell(S^\ell - u_\ell) - \rho_r u_r(S^r - u_r)}{\rho_\ell(S^\ell - u_\ell) - \rho_r(S^r - u_r)}, \tag{17}$$

where $\Delta p \equiv p_r - p_\ell$. The middle states $q^{\star\ell}$, $q^{\star r}$ are obtained by using the conditions above:

$$q^{\star\iota} = \rho_\iota \frac{S^\iota - u_\iota}{S^\iota - S^\star} \begin{pmatrix} 1 \\ S^\star \\ v_\iota \\ \frac{E_\iota}{\rho_\iota} + (S^\star - u_\iota)\left(S^\star + \frac{p_\iota}{\rho_\iota(S^\iota - u_\iota)}\right) \end{pmatrix}, \tag{18}$$

$\iota = \ell, r$. Finally, a definition for the wave speeds must be provided, see e.g. [43, 3]. For the numerical experiments presented in this article we have adopted the following classical simple definition proposed by Davis [9]:

$$S^\ell = \min(u_\ell - c_\ell\,,\, u_r - c_r) \qquad \text{and} \qquad S^r = \max(u_\ell + c_\ell\,,\, u_r + c_r). \tag{19}$$

3.3. A new formulation of the HLLC solver. We illustrate in this Section a novel formulation of the HLLC solver that allows us to highlight a mathematical similarity with the Roe solver. First we introduce two quantities $\check{c}^\ell$, $\check{c}^r$ representing the speeds of sound associated to the external acoustic waves by defining:

$$S^\ell = u_\ell - \check{c}^\ell \qquad \text{and} \qquad S^r = u_r + \check{c}^r. \tag{20}$$

For any given choice of the estimates of the wave speeds S^ℓ and S^r (for example Davis' estimates [9] or Einfeldt's estimates [12]) the relations above determine $\check{c}^\ell$ and $\check{c}^r$. Note that the Davis' choice of S^ℓ and S^r in (19) implies:

$$\check{c}^\ell = \max(c_\ell\,,\, c_r - \Delta u) \qquad \text{and} \qquad \check{c}^r = \max(c_r\,,\, c_\ell - \Delta u), \tag{21}$$

where $\Delta u \equiv u_r - u_\ell$. The speed $S^\star$ can be easily rewritten in terms of $\check{c}^\ell$ and $\check{c}^r$:

$$S^\star = \frac{\rho_\ell \check{c}^\ell u_\ell + \rho_r \check{c}^r u_r - \Delta p}{\rho_\ell \check{c}^\ell + \rho_r \check{c}^r}. \tag{22}$$

The densities $\rho^{\star\iota}$, $\iota = \ell, r$, corresponding to the middle states can be expressed as

$$\rho^{\star\ell} = \rho_\ell \frac{\check{c}^\ell}{S^\star - u_\ell + \check{c}^\ell} \qquad \text{and} \qquad \rho^{\star r} = \rho_r \frac{\check{c}^r}{u_r - S^\star + \check{c}^r}. \tag{23}$$

Then, after some manipulations, we easily see that the HLLC waves for the Euler equations (based on (18)) can be equivalently rewritten as

$$\mathcal{W}^1 = \check{\zeta}_1 \check{r}_1, \quad \mathcal{W}^2 = \check{\mathcal{W}}^2 + \check{\mathcal{W}}^2_s, \;\; \check{\mathcal{W}}^2_s = \check{\zeta}_{2s} \check{r}_{2s}, \quad \mathcal{W}^3 = \check{\zeta}_3 \check{r}_3, \tag{24a}$$

where

(24b)
$$\check{\zeta}_1 = \frac{\rho^{\star\ell}}{\rho_\ell \check{c}^{\,\ell} + \rho_r \check{c}^{\,r}}\left(\frac{\Delta p}{\check{c}^{\,\ell}} - \rho_r \frac{\check{c}^{\,r}}{\check{c}^{\,\ell}}\Delta u\right), \quad \check{\zeta}_3 = \frac{\rho^{\star r}}{\rho_\ell \check{c}^{\,\ell} + \rho_r \check{c}^{\,r}}\left(\frac{\Delta p}{\check{c}^{\,r}} + \rho_\ell \frac{\check{c}^{\,\ell}}{\check{c}^{\,r}}\Delta u\right), \quad \check{\zeta}_{2s} = \check{\rho}\Delta v,$$

$\check{\rho} \equiv \frac{\rho^{\star\ell}+\rho^{\star r}}{2}$, $\Delta v \equiv v_r - v_\ell$, and

(24c)
$$\check{r}_1 = \begin{pmatrix} 1 \\ u_\ell - \check{c}^{\,\ell} \\ v_\ell \\ H_\ell - S^\star \check{c}^{\,\ell} \end{pmatrix}, \quad \check{r}_3 = \begin{pmatrix} 1 \\ u_r + \check{c}^{\,r} \\ v_r \\ H_r + S^\star \check{c}^{\,r} \end{pmatrix}, \quad \check{\mathcal{W}}^2 = \begin{pmatrix} \check{\zeta}_2 \\ \check{\zeta}_2\, S^\star \\ \check{\zeta}_2 \bar{v} \\ \Delta E_n^\star \end{pmatrix}, \quad \check{r}_{2s} = \begin{pmatrix} 0 \\ 0 \\ 1 \\ \bar{v} \end{pmatrix},$$

with

(24d)
$$\check{\zeta}_2 = \rho^{\star r} - \rho^{\star\ell} = \Delta\rho - \left(\left(\frac{\rho^{\star\ell}}{\check{c}^{\,\ell}} + \frac{\rho^{\star r}}{\check{c}^{\,r}}\right)\Delta p + \left(\rho_\ell \rho^{\star r}\frac{\check{c}^{\,\ell}}{\check{c}^{\,r}} - \rho_r \rho^{\star\ell}\frac{\check{c}^{\,r}}{\check{c}^{\,\ell}}\right)\Delta u\right)\frac{1}{\rho_\ell \check{c}^{\,\ell} + \rho_r \check{c}^{\,r}},$$

and

(24e)
$$\Delta E_n^\star = \rho^{\star r} h_r - \rho^{\star\ell} h_l - \Delta p + \check{\zeta}_2\left(\frac{(S^\star)^2}{2} + \overline{\left(\frac{v^2}{2}\right)}\right) + \frac{1}{2}\rho^{\star r}(u_r - S^\star)^2 - \frac{1}{2}\rho^{\star\ell}(u_\ell - S^\star)^2.$$

Above we have denoted with $H = h + \frac{|\vec{u}|^2}{2}$ the total specific enthalpy and we have used the average operator $\bar{(\cdot)} \equiv \frac{(\cdot)_\ell + (\cdot)_r}{2}$. The expressions of the HLLC waves in this novel form reveal analogies with the waves of the Roe solver (see Roe eigenstructure in Appendix A). In particular, the vectors $\check{r}_{1,3}$ and $\check{r}_{2s}$, like the Roe eigenvectors $\hat{r}_{1,4}$ and $\hat{r}_3$, have the form of the eigenvectors of the Euler system associated to the acoustic fields, $r_{1,4}(q) = [1, u \mp c, v, H \mp uc]^{\mathrm{T}}$, and to the shear wave, $r_3(q) = [0, 0, 1, v]^{\mathrm{T}}$, evaluated in a special state that is a function of the left and right Riemann data (although not in the form $\hat{r}_k = r_k(\hat{q})$ as for the Roe solver). The strengths of the waves $\check{\zeta}_{1,3}$ and $\check{\zeta}_{2s}$ have also expressions in terms of pressure and velocity jumps Δp, Δu, Δv, similar to the Roe wave strengths $\hat{\zeta}_{1,4}$ and $\hat{\zeta}_3$, respectively. See also the structure of the two solvers written in a common framework in Appendix B. We may also write the second wave of the HLLC solver as

(25)
$$\check{\mathcal{W}}^2 = \check{\zeta}^2 \check{r}_2, \quad \text{where} \quad \check{r}_2 = \begin{pmatrix} 1 \\ S^\star \\ \bar{v} \\ \Delta e^\star + \frac{(S^\star)^2}{2} + \overline{\left(\frac{v^2}{2}\right)} \end{pmatrix},$$

with

(26)
$$\Delta e^\star = \frac{1}{\rho^{\star r} - \rho^{\star\ell}}\left(\rho^{\star r} h_r - \rho^{\star\ell} h_l - \Delta p + \frac{1}{2}\rho^{\star r}(u_r - S^\star)^2 - \frac{1}{2}\rho^{\star\ell}(u_\ell - S^\star)^2\right).$$

We can observe an analogy of the vector $\check{r}_2$ with the Roe eigenvector $\hat{r}_2$ and with the eigenvector of $A(q)$ associated to the contact wave, $r_2(q) = [1, u, v, \frac{u^2+v^2}{2} - \frac{\chi}{\kappa}]^{\mathrm{T}}$, except for the last component of the vector. If $q_\ell = q_r = q$ then there is a singularity for the quantity $\Delta e^\star$ in (26), so that we can have consistency of $\check{r}_2$ with the eigenvector $r_2(q)$ only if we assume that $\Delta e^\star \to \frac{\partial \mathcal{E}(p,\rho)}{\partial \rho} = -\frac{\chi}{\kappa}$ as $q_{\ell,r} \to q$. Note that clearly if $q_\ell = q_r = q$ the HLLC waves $\mathcal{W}^l$, $l = 1, \ldots, 3$ are simply zero, so that the HLLC Riemann solution structure is always

well determined, as well as the fluctuations of the algorithm. The singularity associated to $\check{r}^2$ computationally does not pose any problem if we use directly the wave $\check{\mathcal{W}}^2$ in (24c). We can also compare the density jump $\check{\zeta}_2$ of the HLLC solver across the contact wave with the density jump $\hat{\zeta}_2$ of the Roe solver, and notice for the solvers analogous terms in $\Delta\rho$ and Δp, but a dependence on Δu only for the HLLC coefficient $\check{\zeta}_2$. If the matrix $\check{R} = [\check{r}_1, \check{r}_2, \check{r}_{2s}, \check{r}_3]$ is nonsingular we can also observe that we can interpret the Riemann solution of the HLLC solver as the Riemann solution of a linearized system with a constant coefficient matrix $\check{A} = \check{A}(q_\ell, q_r)$. The matrix $\check{A}$ can be identified as $\check{A} = \check{R}\check{\Lambda}\check{R}^{-1}$, where $\check{\Lambda} = \mathrm{diag}(u_\ell - \check{c}^\ell, S^\star, S^\star, u_r + \check{c}^r)$. The viscosity matrix of the HLLC scheme is then identified as $\Theta = |\check{A}|$.

To conclude this section, let us note that the reformulation of the HLLC solver presented here for the Euler equations can be also obtained in a similar form for related flow models. In particular in [33] we have shown an analogous reformulation of a HLLC-type solver for a two-phase compressible flow model belonging to the class of models stemming from the one of Baer–Nunziato [1].

4. Application: low Mach number preconditioning techniques. As indicated in the Introduction, the new formulation of the HLLC solver might be advantageous to extend to the HLLC method some algorithms conceived for the Roe's method. Here we provide as an example the design of low Mach number preconditioning techniques for the HLLC scheme on the basis of ideas proposed for the Roe's scheme.

First, let us recall that it is well known that upwind schemes for compressible flow models experience several difficulties as the Mach number vanishes. Here we consider in particular the problem of loss of accuracy of standard schemes at low Mach number related to the spatial discretization of the convective terms of the model equations. This problem has been studied in depth by Guillard and co-workers in a series of papers [19, 17, 16, 18]. Guillard and Viozat in [19] explain via an asymptotic analysis that the loss of accuracy at low Mach number is linked to the generation in the discrete solutions of pressure fluctuations of the wrong order of magnitude in the Mach number, with respect to the behavior of the continuous flow model. The analysis employs a classical procedure based on the non-dimensionalization of the Euler equations and expansions in powers of a reference Mach number M_* for all the variables, of the form:

$$(\cdot) = (\cdot)^{[0]} + (\cdot)^{[1]} M_* + (\cdot)^{[2]} M_*^2 + \dots . \tag{27}$$

Well-prepared initial conditions are assumed, that is $p(\vec{x}, 0) = p_0 + O(M_*^2)(\vec{x})$ and $\vec{u}(\vec{x}, 0) = \vec{u}_0(\vec{x}) + O(M_*)(\vec{x})$, with $\nabla \cdot \vec{u}_0 = 0$. Then one obtains that for solutions of the continuous flow model the pressure can be written as a thermodynamic pressure constant in space plus perturbations of order M_*^2:

$$p(\vec{x}, t) = \mathcal{P}^{[0]}(t) + p^{[2]}(\vec{x}, t) M_*^2 + \dots . \tag{28}$$

In contrast with this result for the continuous model, upwind space discretizations of the Euler equations generate pressure fluctuations of order M_*. This can be shown by using an analogous procedure as for the continuous model, by using asymptotic expansions of the variables in the discrete equations. This analysis is presented in Guillard–Viozat [19] for the Roe's scheme. In the next section we generalize it to the HLLC scheme, by exploiting the reformulation of the HLLC solver introduced in subsection 3.3.

4.1. Roe and HLLC discrete equations at low Mach number. We consider the semi-discrete equations in two dimensions (3) on a Cartesian grid. For simplicity we assume $\Delta x = \Delta y \equiv \delta$. To write the discrete equations in a more compact form as in [19] we use the index $J = (i, j)$ to indicate the grid cell (i, j), and we introduce the index set for neighboring

cells $\nu(J) = \{(i-1,j),(i+1,j),(i,j-1),(i,j+1)\}$. Moreover, we define the jump operator $\Delta_{JK}(\cdot) \equiv (\cdot)_J - (\cdot)_K$ that expresses the difference between values at the reference cell J and its neighboring cell K, and we denote with $(\cdot)_{JK}$ quantities corresponding to interfaces between cells J and K. We use $\vec{n}_{JK} = (n_x, n_y)_{JK}$ to denote the unit normal vector to the interface JK, from cell J to cell K, and the transverse unit vector is then $\vec{n}^{\perp}_{JK} = (-n_y, n_x)_{JK}$. We indicate the normal and transverse components of $\vec{u} = (u, v)$ with $U = \vec{u} \cdot \vec{n}$ and $V = \vec{u} \cdot \vec{n}^{\perp}$, respectively. As a first step we write the non-dimensionalized semi-discrete equations for both the two-dimensional Roe's scheme and the HLLC scheme in a unified formulation. The equations are reported in Appendix B. Next, we expand all the variables in powers of the reference Mach number M_*, as for the continuous case (27). Collecting terms with equal powers of M_*, one obtains at order M_*^{-2} from the momentum equation (51):

$$\sum_{K\in\nu(J)} \left(p_K^{[0]}\, \vec{n}_{JK} + \frac{1}{2}\left(\frac{c_{JK}^{K[0]}}{\tilde{c}_{JK}^{K[0]}} - \frac{c_{JK}^{J[0]}}{\tilde{c}_{JK}^{J[0]}} \right) \vec{n}_{JK} \Delta_{JK} p^{[0]} \right) = 0, \tag{29}$$

where the interfaces quantities $(\cdot)_{JK}^{J,K}$ for the Roe and HLLC solvers are specified in Appendix B in (47), (48), (49). At order M_*^{-1} from the mass equation (50) we have

$$\sum_{K\in\nu(J)} \left(\frac{1}{\tilde{c}_{JK}^{J[0]}} + \frac{1}{\tilde{c}_{JK}^{K[0]}} \right) \Delta_{JK} p^{[0]} = 0, \tag{30}$$

and from the energy equation (52):

$$\sum_{K\in\nu(J)} \left(\frac{H_{JK}^{J[0]}}{\tilde{c}_{JK}^{J[0]}} + \frac{H_{JK}^{K[0]}}{\tilde{c}_{JK}^{K[0]}} \right) \Delta_{JK} p^{[0]} = 0. \tag{31}$$

We notice that $p_J^{[0]} = \text{constant}\ \forall J$ is a common solution of the equations (29), (30), (31). We also observe that the coefficients multiplying $\Delta_{JK} p^{[0]}$ in (30) and (31) are positive, hence a discrete maximum principle applies, and the extrema of the pressure field $p^{[0]}$ must be on the boundary. Assuming suitable boundary conditions we can conclude that the solution $p^{[0]} =$ constant is also unique. This is the case in particular if we assume that the pressure on the boundary is a constant p_0 (up to fluctuations of order M_*^2) [19]. Now, let us consider this case $p_J^{[0]} = \text{constant}\ \forall J$, and let us use this result in the next order equations. In particular, the momentum equation (51) at order M_*^{-1} gives

$$\sum_{K\in\nu(J)} \left(p_K^{[1]}\, \vec{n}_{JK} + \frac{1}{2}\left(\frac{c_{JK}^{K[0]}}{\tilde{c}_{JK}^{K[0]}} - \frac{c_{JK}^{J[0]}}{\tilde{c}_{JK}^{J[0]}} \right) \vec{n}_{JK} \Delta_{JK} p^{[1]} + \frac{1}{2}\left(\frac{\rho_{JK}^{J[0]} (c_{JK}^{J[0]})^2}{\tilde{c}_{JK}^{J[0]}} + \frac{\rho_{JK}^{K[0]} (c_{JK}^{K[0]})^2}{\tilde{c}_{JK}^{K[0]}} \right) \vec{n}_{JK} \Delta_{JK} U^{[0]} \right) = 0. \tag{32}$$

In general this equation admits non-constant solutions for the order 1 pressure $p^{[1]}$ [19, 37]. Therefore we conclude that solutions of the discrete equations for the Roe and HLLC solvers contain perturbations of order M_*: $p(\vec{x}, t) = p_0 + p^{[1]}(\vec{x}, t) M_* + \ldots$, in contrast with the results for the continuous model (28). Nonetheless, we have to recall that for the special case of triangular meshes the solution of the discrete equations of the Roe solver for the pressure $p^{[1]}$ can be indeed $p_J^{[1]} = \text{constant}\ \forall J$, and for such grids the accuracy problem might not appear. We refer the reader to [37, 11, 16] for details.

4.2. Preconditioning of the numerical dissipation term. A well known strategy to cure the loss of accuracy of finite volume Godunov-type schemes for the Euler equations as the Mach number approaches zero consists in correcting the numerical dissipation term $\mathcal{V}\Delta Q_{i+1/2}$ in the numerical fluxes (9). This approach alters the order of magnitude of the entries of this term with respect to the Mach number so that the resulting discrete scheme recovers a low Mach number asymptotic behavior consistent with the one of the continuous model. For several methods proposed in the literature the low Mach number correction is obtained by applying a preconditioning matrix P to the viscosity matrix $\Theta_{i+1/2}$ of the scheme [8, 45, 47, 46, 19]. We will denote with $\mathcal{V}^P\Delta Q_{i+1/2}$ the corrected (preconditioned) dissipation term that replaces the original one $\mathcal{V}\Delta Q_{i+1/2}$ in the numerical fluxes (9), or, equivalently, in the fluctuations (10). Note that the class of preconditioning strategies that we consider here alters only dissipative contributions, while the temporal term and the centered flux are unchanged. Therefore, as noted in [19], the preconditioned numerical scheme remains a conservative time-consistent approximation of the Euler equations. As we will see in the next subsections, for the preconditioning schemes considered in the present work, we can interpret the low Mach number correction as a modification of the waves and speeds of the Riemann solver that contribute to the numerical viscosity term, and the preconditioned dissipation term has the form (cf. (11))

$$\mathcal{V}^P\Delta Q_{i+1/2} = \sum_{l=1}^{\mathscr{M}} |s^{lP}_{i+1/2}|\mathcal{W}^{lP}_{i+1/2}\,, \tag{33}$$

where s^{lP} and $\mathcal{W}^{lP}$, $l = 1,\dots,\mathscr{M}$, are preconditioned waves and speeds. Preconditioning techniques have been extensively developed especially for the Roe's scheme [19, 41, 10, 27, 29, 28, 36, 16, 18]. These techniques typically correct at low Mach number the acoustic waves and/or speeds of the Roe solver, see in particular some reviews in [28, 18]. For instance the simple low Mach number fix of Rieper (LMRoe scheme) [36] corrects the Roe wave strengths $\hat{\zeta}_{1,4}$ by replacing the jump of the normal velocity Δu as:

$$\Delta u \quad \rightarrow \quad \Delta u^P = \min(\tilde{M}, 1)\Delta u, \tag{34}$$

where $\tilde{M}$ is a local Mach number computed by using the data of the local Riemann problem. The All-speed Roe scheme of Li and Gu [27] consists in a correction of the Roe eigenvalues, while the Roe-Turkel scheme of Guillard–Viozat [19], recalled more in detail below, modifies the Roe eigenvalues $\hat{\lambda}_{1,4}$, the Roe eigenvectors $\hat{r}_{1,4}$ and the corresponding wave strengths $\hat{\zeta}_{1,4}$. Preconditioned techniques for the HLLC scheme are more scarce, e.g. [31, 23]. Existing methods typically modify the speeds S^ℓ, S^r of the standard solver by employing corrections analogous to those used in some of the preconditioning methods for the Roe solver. The corrected values of S^ℓ, S^r are used in all the formulas of the HLLC Riemann structure, this implying a correction of the speed S^* and of all the waves of the solver. Although these preconditioned methods for HLLC-type schemes have been shown to produce good numerical results, they seem to lack rigorous asymptotic analyses. The novel form of the HLLC solver that we have highlighted allows us to easily extend strategies and analysis methods used for the Roe solver to the family of HLLC-type solvers. For instance, the fix of Rieper is immediately extended to the HLLC method by using the modified velocity jump in (34) to correct the strengths $\check{\zeta}_{1,3}$ (24b) of the acoustic waves of the HLLC solver. Here we will detail in particular the application of our idea to the Roe-Turkel method of Guillard–Viozat [19] and illustrate a new HLLC-Turkel scheme. Indeed, based on our experience, and also for instance on the review [18], the method of Guillard–Viozat is one of the most effective.

4.3. The Roe-Turkel method for the Euler equations. The Roe-Turkel scheme of [19] is a correction of the classical Roe's method obtained by applying Turkel's preconditioner

[45, 46] to the Roe dissipation term in (13). Here the Roe viscosity matrix $\Theta_{i+1/2} = |\hat{A}_{i+1/2}|$ is replaced by the preconditioned version

$$\Theta^P_{i+1/2} = P^{-1}_{i+1/2}|P_{i+1/2}\hat{A}_{i+1/2}|, \tag{35}$$

where P is Turkel's preconditioning matrix. This matrix for the Euler equations is defined on the basis of the entropic variables $\varphi = [p, \vec{u}, s]^{\mathrm{T}}$, where s denotes the entropy, as

$$P^{\varphi} = \mathrm{diag}(\beta^2, I_d, 1). \tag{36}$$

Here I_d denotes the identity matrix $\in \mathbb{R}^{d\times d}$, and d indicates the spatial dimension. The parameter $\beta \leq 1$ is of the order of the local Mach number $M_{i+1/2}$ if $M_{i+1/2} \leq 1$, and equal to 1 otherwise. It can be set for instance at each interface as $\beta_{i+1/2} = \min(\max(\epsilon, M_{i+1/2}), 1)$, where $0 < \epsilon \ll 1$. The tolerance ϵ is used to avoid the singularity of the preconditioned quantities that may occur for $|\vec{u}| = 0$. More efficient definitions of β can be used to deal with stagnation points, see e.g. [7]. The local Mach number $M_{i+1/2}$ can be computed by using the Roe averages as $M_{i+1/2} = M_{\ell r} = \frac{|\vec{\hat{u}}|}{\hat{c}}$. Turkel's preconditioner in terms of the conserved variables q is then obtained as $P(q) = \frac{\partial q}{\partial \varphi} P^{\varphi} \frac{\partial \varphi}{\partial q}$. For the plane-wave Riemann problem considered here we have $d = 2$, and $\varphi = [p, u, v, s]^{\mathrm{T}}$. The resulting numerical dissipation term of the Roe-Turkel scheme is found as (cf. [19])

$$\mathcal{W}^P \Delta Q_{i+1/2} = P^{-1}_{i+1/2}|P_{i+1/2}\hat{A}_{i+1/2}|(q_{i+1} - q_i) = \sum_{l=1}^{4} (\hat{\zeta}^P_l |\hat{\lambda}^P_l| \tilde{\hat{r}}^P_l)_{i+1/2}\,, \tag{37}$$

where $\tilde{\hat{r}}^P_l = P^{-1}\hat{r}^P_l$, and $\hat{\lambda}^P_l, \hat{r}^P_l, l = 1, \ldots, 4$, are the eigenvalues and eigenvectors, respectively, of the matrix $P\hat{A}$. The coefficients $\hat{\zeta}^P_l$ are obtained by projecting the jump Δq onto the basis of the eigenvectors $\hat{r}^P_l$ as $\Delta q = \sum_{l=1}^4 \hat{\zeta}^P_l \hat{r}^P_l$. The preconditioned waves and speeds of the Roe-Turkel scheme to be used in (33) are then $\mathcal{W}^{lP} = \hat{\zeta}^P_l \tilde{\hat{r}}^P_l$ and $s^{lP} = \hat{\lambda}^P_l, \quad l = 1, \cdots, 4$. Based on the results derived in [19], the acoustic waves, which correspond to the first and fourth characteristic fields, are modified as follows when Turkel's preconditioning is applied to the Roe's scheme:

$$\hat{\lambda}_{1,4} = \hat{u} \mp \hat{c} \;\rightarrow\; \hat{\lambda}^P_{1,4} = \tfrac{1}{2}(1+\beta^2)\hat{u} \mp \tfrac{1}{2}\sqrt{X_\beta}, \tag{38a}$$

$$\hat{r}_{1,4} = \begin{pmatrix} 1 \\ \hat{u} \mp \hat{c} \\ \hat{v} \\ \hat{H} \mp \hat{u}\hat{c} \end{pmatrix} \rightarrow \tilde{\hat{r}}^P_{1,4} = \begin{pmatrix} 1 \\ \hat{u} + (\hat{\lambda}^P_{1,4} - \hat{u}\beta^2) \\ \hat{v} \\ \hat{H} + \hat{u}(\hat{\lambda}^P_{1,4} - \hat{u}\beta^2) \end{pmatrix}, \tag{38b}$$

$$\hat{\zeta}_{1,4} = \tfrac{1}{2\hat{c}}\left(\tfrac{\Delta p}{\hat{c}} \mp \hat{\rho}\Delta u\right) \rightarrow \hat{\zeta}^P_{1,4} = \tfrac{1}{\sqrt{X_\beta}}\left(\tfrac{\Delta p}{\mp(\hat{\lambda}^P_{1,4} - \hat{u}\beta^2)} \mp \hat{\rho}\Delta u\right), \tag{38c}$$

with

$$X_\beta = ((1-\beta^2)\hat{u})^2 + (2\beta\hat{c})^2. \tag{38d}$$

As a consequence of the form of the preconditioner (36), the wave structure corresponding to the second and third characteristic fields associated to the eigenvalue $\hat{\lambda}_2 = \hat{\lambda}_3 = \hat{u}$ (contact wave) is unchanged with respect to the method with no preconditioning (see Roe wave structure in Appendix A): $\hat{\lambda}^P_l = \hat{\lambda}_l = \hat{u}$, $\tilde{\hat{r}}^P_l = \hat{r}_l$, $\hat{\zeta}^P_l = \hat{\zeta}_l$, $l = 2, 3$, hence $s^{lP} = s^l$ and $\mathcal{W}^{lP} = \mathcal{W}^l$ for $l = 2, 3$.

4.4. A novel HLLC-Turkel method for the Euler equations. We present in this section a new preconditioning technique for the HLLC scheme for the Euler equations, which extends the strategy of the Roe-Turkel scheme of Guillard–Viozat [19]. The idea is to exploit the formal similarity of the wave structure of the HLLC Riemann solver with the one of the Roe solver, which we have highlighted in subsection 3.3. By analogy with the preconditioned wave structure of the Roe-Turkel method (38) we propose the following low Mach number correction of the acoustic waves and speeds of the HLLC method:

$$S^{\ell} = u_\ell - \check{c}^{\,\ell} \;\to\; S^{\ell P} = \tfrac{1}{2}(1+\beta^2)u_\ell - \tfrac{1}{2}\sqrt{X_{\beta\ell}} \tag{39a}$$

$$S^{r} = u_r + \check{c}^{\,r} \;\to\; S^{rP} = \tfrac{1}{2}(1+\beta^2)u_r + \tfrac{1}{2}\sqrt{X_{\beta r}} \tag{39b}$$

$$\check{r}_1 = \begin{pmatrix} 1 \\ u_\ell - \check{c}^{\,\ell} \\ v_\ell \\ H_\ell - S^\star \check{c}^{\,\ell} \end{pmatrix} \to \check{r}_1^P \begin{pmatrix} 1 \\ u_\ell + (S^{\ell P} - u_\ell\beta^2) \\ v_\ell \\ H_\ell + S^\star(S^{\ell P} - u_\ell\beta^2) \end{pmatrix} \tag{39c}$$

$$\check{r}_3 = \begin{pmatrix} 1 \\ u_r + \check{c}^{\,r} \\ v_r \\ H_r + S^\star \check{c}^{\,r} \end{pmatrix} \to \check{r}_3^P = \begin{pmatrix} 1 \\ u_r + (S^{rP} - u_r\beta^2) \\ v_r \\ H_r + S^\star(S^{rP} - u_r\beta^2) \end{pmatrix} \tag{39d}$$

(39e)
$$\check{\zeta}_1 = \frac{\rho^{\star\ell}}{\rho_\ell \check{c}^{\,\ell} + \rho_r \check{c}^{\,r}} \left(\frac{\Delta p}{\check{c}^{\,\ell}} - \rho_r \frac{\check{c}^{\,r}}{\check{c}^{\,\ell}} \Delta u \right) \to \check{\zeta}_1^P = \frac{\rho^{\star\ell}}{\rho_\ell \frac{\sqrt{X_{\beta\ell}}}{2} + \rho_r \frac{\sqrt{X_{\beta r}}}{2}} \left(\frac{\Delta p}{-(S^{\ell P} - u_\ell\beta^2)} - \rho_r \frac{\check{c}^{\,r}}{\check{c}^{\,\ell}} \Delta u \right)$$

(39f)
$$\check{\zeta}_3 = \frac{\rho^{\star r}}{\rho_\ell \check{c}^{\,\ell} + \rho_r \check{c}^{\,r}} \left(\frac{\Delta p}{\check{c}^{\,r}} + \rho_\ell \frac{\check{c}^{\,\ell}}{\check{c}^{\,r}} \Delta u \right) \to \check{\zeta}_3^P = \frac{\rho^{\star r}}{\rho_\ell \frac{\sqrt{X_{\beta\ell}}}{2} + \rho_r \frac{\sqrt{X_{\beta r}}}{2}} \left(\frac{\Delta p}{S^{rP} - u_r\beta^2} + \rho_\ell \frac{\check{c}^{\,\ell}}{\check{c}^{\,r}} \Delta u \right)$$

where

$$X_{\beta\ell} = ((1-\beta^2)u_\ell)^2 + (2\beta\check{c}^{\,\ell})^2 \qquad \text{and} \qquad X_{\beta r} = ((1-\beta^2)u_r)^2 + (2\beta\check{c}^{\,r})^2. \tag{39g}$$

The parameter β is defined as indicated in the previous section by using a local Mach number that can be computed for instance as $M_{i+1/2} = M_{\ell r} = \min\left(\frac{|\vec{u}_\ell|}{\check{c}^{\,\ell}}, \frac{|\vec{u}_r|}{\check{c}^{\,r}}\right)$. The preconditioned acoustic waves and speeds to be used in (33) are then $\mathcal{W}^{1,3P} = \check{\zeta}_{1,3}^P \check{r}_{1,3}^P$, $s^{1,3P} = S^{\ell,rP}$. As for the Roe-Turkel method, we maintain unaltered the contact wave:

$$s^{2P} = S^\star, \quad \mathcal{W}^{2P} = \check{\mathcal{W}}^2 + \check{\mathcal{W}}_s^2. \tag{40}$$

This correction of the HLLC method produces a rescaling of contributions to the numerical dissipation term with respect to the Mach number that is analogous to the one of the Roe-Turkel method. This is discussed further in the next section.

Before proceeding, let us remark, as we pointed out in the Introduction, that we have extended in [33] the HLLC-Turkel scheme presented here to a two-phase compressible flow model, and indeed the present investigation originated from our interest in computational multiphase flow models applicable to a wide range of Mach number regimes.

4.5. Roe and HLLC preconditioned discrete equations. From the form of the preconditioned waves and speeds of the Roe solver (38) and of the HLLC solver (39) we observe that the speed of sound appearing in the original acoustic waves is replaced by quantities that are of the order of the flow velocity. This alters the order of the contributions of these waves to the

numerical dissipation term. As noted in [19] for the Roe-Turkel scheme, with respect to the original semi-discrete equations reported in Appendix B, the application of preconditioning leads to dissipation terms of order M_*^{-2} in the mass and energy equations, and the dissipative terms of order M_*^{-1} disappear in all the equations. The preconditioned waves are written in a unified formulation for the Roe and HLLC solvers in (53), (54) in Appendix B. By employing these waves and by using as before expansions in powers of M_* in the non-dimensionalized discrete equations, we find at order M_*^{-2} for the mass, momentum and energy equations:

(41a)
$$\sum_{K\in\mathcal{V}(J)}\left(\frac{1}{\tilde{c}_{JK}^{J\,P[0]}}+\frac{1}{\tilde{c}_{JK}^{K\,P[0]}}\right)\Delta_{JK}p^{[0]}=0,$$

(41b)
$$\sum_{K\in\mathcal{V}(J)}\left(p_K^{[0]}\vec{n}_{JK}+\frac{1}{2}\left(\frac{2\vec{u}_{JK}^{J[0]}+U_{JK}^{J[0]}\vec{n}_{JK}}{\tilde{c}_{JK}^{J\,P[0]}}+\frac{2\vec{u}_{JK}^{K[0]}+U_{JK}^{K[0]}\vec{n}_{JK}}{\tilde{c}_{JK}^{K\,P[0]}}+\left(\frac{c_{JK}^{K\,P[0]}}{\tilde{c}_{JK}^{K\,P[0]}}-\frac{c_{JK}^{J\,P[0]}}{\tilde{c}_{JK}^{J\,P[0]}}\right)\vec{n}_{JK}\right)\Delta_{JK}p^{[0]}\right)=0,$$

(41c)
$$\sum_{K\in\mathcal{V}(J)}\left(\frac{H_{JK}^{J[0]}}{\tilde{c}_{JK}^{J\,P[0]}}+\frac{H_{JK}^{K[0]}}{\tilde{c}_{JK}^{K\,P[0]}}\right)\Delta_{JK}p^{[0]}=0,$$

where, based on the definition of $\tilde{c}_{JK}^{J,K\,P}$ in (54), $\tilde{c}_{JK}^{J,K\,P[0]}=c_{JK}^{J,K\,P[0]}$ for the Roe solver, and $\tilde{c}_{JK}^{J,K\,P[0]}=\frac{\rho_J^{[0]}c_{JK}^{J\,P[0]}+\rho_K^{[0]}c_{JK}^{K\,P[0]}}{2\rho_{JK}^{\star\,J,K[0]}}$ for the HLLC solver, and we have, based on (53),

(41d)
$$c_{JK}^{J,K\,P[0]}=\frac{1}{2}\sqrt{X_{\tilde{\beta},JK}^{J,K[0]}}=\frac{1}{2}\sqrt{\left(U^{J,K[0]}\right)^2+\left(2\tilde{\beta}c^{J,K[0]}\right)^2},$$

with $\tilde{\beta}=\frac{\beta}{M_*}$. Non-preconditioned interface quantities $(\cdot)_{JK}^{J,K}$ are specified in (48), (49). We can now use the arguments detailed in [19] to conclude that under reasonable assumptions on the boundary conditions, and specifically under the assumption of pressure equal to a constant p_0 (up to fluctuations of order M_*^2), the discrete equations with preconditioned dissipation of the Roe-Turkel and HLLC-Turkel schemes support pressure perturbations of order M_*^2. The proof is based on the observation that $p^{[0]}=$ constant is a common solution of the equations (41) above, and that the coefficients multiplying $\Delta_{JK}p^{[0]}$ in (41a), (41c) are positive, hence a discrete maximum principle applies and an interior point cannot be an extremum. Moreover, since there are no terms of order M_*^{-1} in the discrete equations with preconditioned dissipation, the equations that we obtain at order M_*^{-1} when we use asymptotic expansions of the variables have the form (41) with $p^{[0]}$ replaced by $p^{[1]}$ [19]. Hence, at the discrete level $p(\vec{x},t)=p_0+p^{[2]}(\vec{x},t)M_*^2+\ldots$, as for the continuous model.

4.6. Numerical experiments. We present in this Section several numerical experiments aimed at showing the effectiveness of the proposed preconditioned HLLC method. Since here we focus on the problem of loss of accuracy at low Mach number related to the spatial discretization of convective terms, we use a simple explicit scheme for integration in time of (3). Note that this implies an extremely severe time step restriction [5] and computationally it is highly expensive. For practical applications time-implicit integrations should be employed, e.g. [4].

4.6.1. Low Mach number channel flow. We perform a channel flow numerical test similar to the one presented in [10] (see also [22] p. 590). We simulate a two-dimensional flow ($\vec{u}=(u,v)$, $\vec{x}=(x,y)$) in a channel of length = 4 m and height = 1 m with a bump

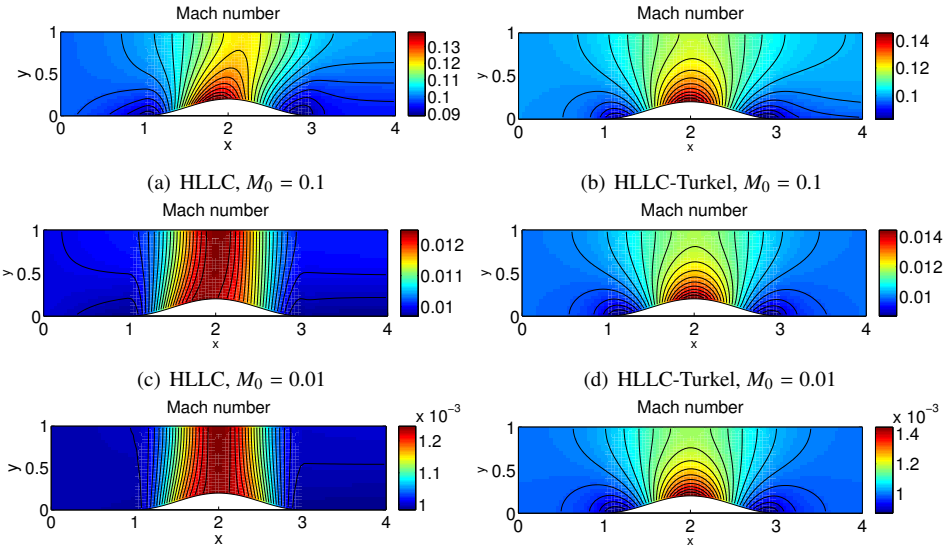

(a) HLLC, $M_0 = 0.1$ (b) HLLC-Turkel, $M_0 = 0.1$

(c) HLLC, $M_0 = 0.01$ (d) HLLC-Turkel, $M_0 = 0.01$

(e) HLLC, $M_0 = 0.001$ (f) HLLC-Turkel, $M_0 = 0.001$

FIG. 2. *Channel flow numerical test. Results for the Mach number obtained with the standard HLLC scheme (left column) and the preconditioned HLLC-Turkel scheme (right column) for the three considered values of the inlet Mach number* M_0.

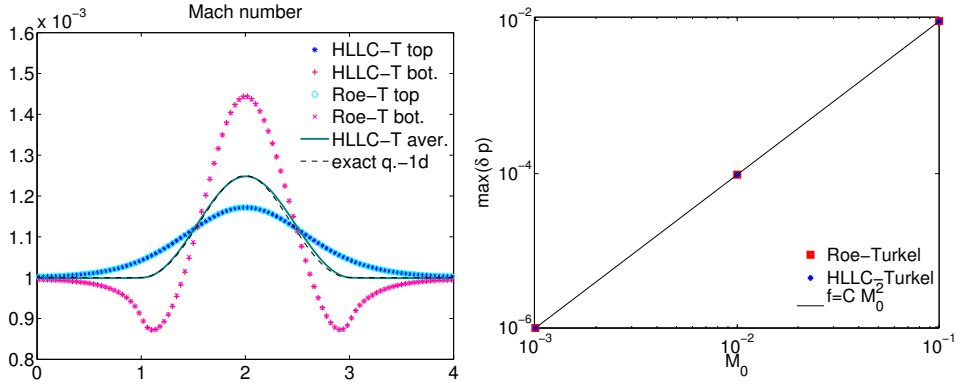

FIG. 3. *Channel flow numerical test. Left: Mach number at the top and bottom boundaries computed by the Roe-Turkel and HLLC-Turkel schemes for the test with* $M_0 = 10^{-3}$*, average Mach number over the channel section computed by the HLLC-Turkel scheme, and exact quasi-one-dimensional steady solution. Right: log-log graph of the maximum pressure fluctuations* $\delta p_{\max}$ *versus the Mach number* $M_* = M_0$ *for the HLLC-Turkel and Roe-Turkel schemes. The reference curve* $f(M_0) = CM_0^2$*, which is a straight line of slope 2 in the log-log graph, is also drawn to observe more easily the behavior of the fluctuations with respect to* M_0*. The constant C is determined so that f passes through the point corresponding to results obtained with the HLLC-Turkel method for the test with* $M_0 = 10^{-2}$.

defined by $y = (1 - \cos((x-1)\pi))/10$, if $x \in [1,3]$, and $y = 0$ otherwise. The fluid is a perfect gas with $\gamma = 1.4$ and $\eta = \varpi = 0$. The computational domain is $[0,4] \times [0,1]\,\mathrm{m}^2$. Initially, we set the pressure and the temperature values to $p_0 = 10^5$ Pa and $T_0 = 288$ K, respectively. The initial specific enthalpy is then $h_0 = 2.8930 \times 10^5$ J/kg. We impose a velocity $\vec{u}_{\mathrm{in}} = (u_{\mathrm{in}}, 0)$, where the horizontal velocity component u_{in} is defined such that the initial Mach number $M_0 = \frac{|\vec{u_0}|}{\sqrt{\gamma p_0/\rho_0}}$ is equal to a desired value M_0. Here we will perform tests

with $M_0 = 10^{-1}, 10^{-2}, 10^{-3}$. Note that initial data are well-prepared, in the sense defined in section 4. At the left inlet boundary we impose the values h_0, u_0. At the right outlet boundary we set the pressure value p_0, while the other flow variables are extrapolated from the interior solution. Top and bottom boundaries are solid walls (slipping boundary condition). We solve the Euler equations by using the standard HLLC scheme, the preconditioned Roe-Turkel scheme of [19] and our new preconditioned HLLC-Turkel scheme. We use a quadrilateral curvilinear grid with 100×25 cells. Pseudo-color plots of the results for the Mach number obtained with the standard HLLC scheme and with the preconditioned HLLC-Turkel scheme are displayed in Figure 2 at a time at which stationary conditions are approximately attained. We can observe the accuracy and convergence difficulties of the HLLC method for these low Mach number tests. The application of Turkel's preconditioning allows us to recover the correct behavior of the solution and good accuracy. In Figure 3 we display the profiles of the Mach number at the top and bottom boundaries obtained with both the Roe-Turkel and the HLLC-Turkel scheme (left plot) for the test case with $M_0 = 10^{-3}$, and we also show the average value of the Mach number over the channel section as computed by the HLLC-Turkel scheme and the exact quasi-one-dimensional steady solution. The results for the Roe-Turkel and HLLC-Turkel method are not distinguishable. This is indeed not surprising considering the similar wave structure of the two solvers (47)-(48)-(49) and the small variations that characterize the solution of these tests. Following [19], to assess the accuracy of the HLLC-Turkel method at low Mach number we compute the maximum pressure fluctuations in the whole flow domain $\delta p_{\max} = \frac{p_{\max} - p_{\min}}{p_0}$ for the set of considered experiments. We display in Figure 3 (right plot) a log-log plot of the values of $\delta p_{\max}$ versus M_0 for the Roe-Turkel and HLLC-Turkel schemes. We can observe that pressure fluctuations produced by the HLLC-Turkel scheme, like those of the Roe-Turkel scheme, correctly scale with the square of the inlet Mach number M_0, consistently with the theoretical results for the continuous flow model.

4.6.2. Gresho vortex problem. We employ here our HLLC-Turkel scheme to simulate the Gresho vortex, a rotating vortex that is a stationary solution of the incompressible Euler equations [15, 30, 32]. The objective is to assess the accuracy of the scheme in maintaining the vortex solution for a low Mach number flow on the discrete grid as time evolves. The problem setup is taken from [32] (see also [20]). The rotating vortex is centered at the point $\vec{x}_C = (0.5, 0.5)$ of the computational domain $[0,1] \times [0,1]$. Initially, at $t = 0$, the density is uniform and equal to $\rho(\vec{x}, 0) = \rho_0 = 1$. The initial conditions for the pressure and the velocity are specified as follows as a function of the distance $r = |\vec{x} - \vec{x}_C|$ from the vortex center:

(42a)
$$p(\vec{x},0) = \begin{cases} p_0 + 12.5r^2 & \text{if} \quad 0 \le r < 0.2, \\ p_0 + 4 - 4\log 0.2 + 12.5r^2 - 20r + 4\log r & \text{if} \quad 0.2 \le r < 0.4, \\ p_0 - 2 + 4\log 2 & \text{if} \quad 0.4 \le r, \end{cases}$$

(42b)
$$u(\vec{x},0) = -u_\phi(r)\sin\phi, \quad v(\vec{x},0) = u_\phi(r)\cos\phi, \quad u_\phi(r) = \begin{cases} 5r & \text{if} \quad 0 \le r < 0.2, \\ 2 - 5r & \text{if} \quad 0.2 \le r < 0.4, \\ 0 & \text{if} \quad 0.4 \le r, \end{cases}$$

with $\tan\phi = \frac{y - y_C}{x - x_C}$. The parameter $p_0 = \frac{\rho_0}{\gamma M_*^2}$, where $\gamma = 1.4$, depends on the desired maximum Mach number M_* of the rotating flow. Here we consider two cases: $M_* = 0.1$, as in [32], and $M_* = 0.01$. We use a grid with 80×80 cells with periodic boundary conditions. We perform computations with the standard HLLC scheme and the HLLC-Turkel scheme. We have also performed several tests with the Roe-Turkel scheme, and no relevant differences

were found with respect to the HLLC-Turkel scheme. Only for this problem we include second-order corrections both to be able to compare our results with those in the literature [32, 20], and to provide an example that indicates that second-order terms alone do not suffice to overcome low Mach number difficulties, cf. also [19]. Second-order corrections in the numerical scheme are expressed in terms of the waves of the Riemann solver, as indicated in (7) (cf. [25]), and a Monotonized Centered (MC) limiter function ϕ is applied. For the HLLC-Turkel and Roe-Turkel methods preconditioned waves are used to define second-order terms. Let us note that instabilities were observed with the wave propagation scheme (3) with second-order corrections (7) if unlimited waves are used ($\phi = 1$) with a Δt for which computations with the MC limiter are stable, both with the non-preconditioned and with the preconditioned schemes (Roe and HLLC). We found that one can overcome this instability problem for the standard Roe's scheme by adding transverse fluctuations [24]. The computation of these transverse contributions uses a projection of the fluctuations onto the Roe eigenvectors, and for the HLLC scheme it is not clear how this fluctuation splitting could be performed. In fact, our novel formulation of the HLLC solver could suggest a way to define transverse fluctuations for the HLLC method in analogy with the Roe solver, nonetheless this aspect is not investigated in the present work. To begin with, we display in Figure 4 first-order results for the test case with $M_* = 0.01$ obtained with the HLLC-Turkel method (subplot (a)), the Roe-Turkel method (subplot (b)), and the standard HLLC method (subplot (c)). The initial condition for the Mach number for this test can be seen in Figure 5, subplot (a). The results obtained with the Roe-Turkel and HLLC-Turkel methods do not show visible differences. These two first-order preconditioned methods introduce a large amount of numerical dissipation and distort the vortex shape. The ratio K_E of the total kinetic energy relative to its initial value is $K_E = 0.3953$ at $t = 2$ for both methods. The standard first-order HLLC scheme produces more dissipation ($K_E = 0.3900$) and, moreover, loses completely the initial circular shape of the vortex. The subplots (b)-(c) of Figure 5 show the Mach number computed by our HLLC-Turkel scheme with second-order corrections at $t = 1$ and $t = 2$ (times corresponding to 1 and 2 rotations of the vortex) for the test with $M_* = 0.01$, and the subplot (d) shows results with the same method for the test with $M_* = 0.1$. We observe the good performance of the HLLC-Turkel method, which preserves very well the circular shape of the vortex for the two considered values of M_*. The results appear qualitatively as accurate as those presented in [32]. Some artificial dissipation is introduced, the loss of kinetic energy is nonetheless small, with the ratio K_E being $K_E = 0.9938$ at $t = 1$ and $K_E = 0.9893$ at $t = 2$ for the test with $M_* = 0.01$ and $K_E = 0.9926$ at $t = 2$ for the test with $M_* = 0.1$. While first-order non-preconditioned results seem not to be affected by a reduction of Δt, the results of the non-preconditioned Roe's and HLLC methods with second-order corrections exhibit better accuracy if the time step is decreased with respect to the largest time step allowed for stability. Here we display results for the second-order HLLC scheme obtained with the same time step used for the HLLC-Turkel scheme, specifically in subplot (e) for the test with $M_* = 0.1$ ($\Delta t = 0.4 \times 10^{-5}$), and in subplot (f) for the test with $M_* = 0.01$ ($\Delta t = 0.4 \times 10^{-6}$). The standard non-preconditioned HLLC scheme with second-order corrections shows significant improvement with respect to first-order results, with the chosen very small Δt. Nonetheless, for the same order of the computational time, it still introduces more numerical dissipation than the preconditioned method, giving at $t = 2$ $K_E = 0.9552$ for the case $M_* = 0.1$ and $K_E = 0.7419$ for the case $M_* = 0.01$.

5. Conclusions. In this work we have presented a novel formulation of the HLLC Riemann solver. This formulation allows us to recognize a formal mathematical similarity of the HLLC solver with the Roe solver. This could be exploited to apply to HLLC-type methods some numerical strategies conceived originally for the Roe's method. We have illustrated

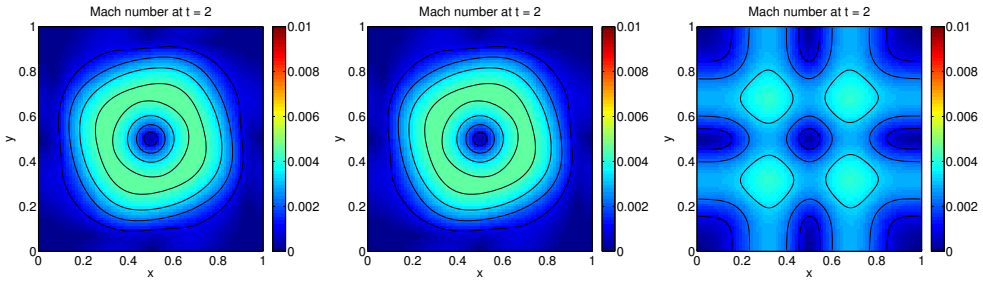

(a) HLLC-Turkel (b) Roe-Turkel (c) HLLC

FIG. 4. *Gresho vortex test with $M_* = 0.01$, first-order results for the Mach number at $t = 2$. (a) HLLC-Turkel scheme; (b) Roe-Turkel scheme; (c) standard HLLC scheme.*

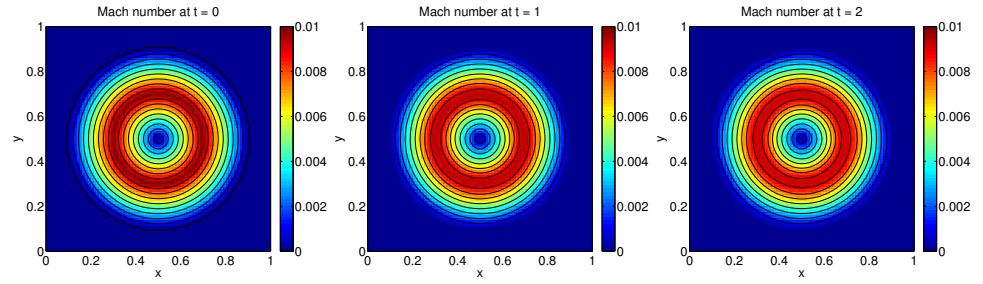

(a) $M_* = 0.01$, $t = 0$ (b) HLLC-Turkel, $M_* = 0.01$, $t = 1$ (c) HLLC-Turkel, $M_* = 0.01$, $t = 2$

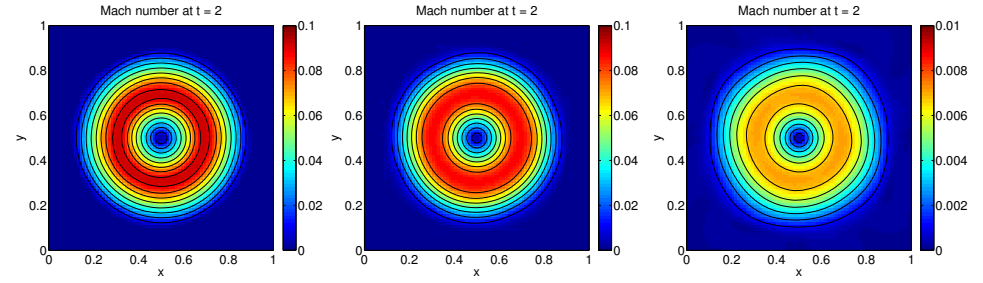

(d) HLLC-Turkel, $M_* = 0.1$, $t = 2$ (e) HLLC, $M_* = 0.1$, $t = 2$ (f) HLLC, $M_* = 0.01$, $t = 2$

FIG. 5. *Gresho vortex test, results with second-order corrections included. (a) Mach number at $t = 0$ for the test with $M_* = 0.01$; (b)-(c): Mach number at $t = 1$ and $t = 2$ computed by the HLLC-Turkel scheme for the test with $M_* = 0.01$; (d): Mach number at $t = 2$ computed by the HLLC-Turkel scheme for the test with $M_* = 0.1$; (e)-(f): Mach number at $t = 2$ computed by the HLLC scheme for the tests with $M_* = 0.1$ and $M_* = 0.01$, respectively.*

an application to the design of low Mach number preconditioning techniques for the HLLC scheme for the Euler equations, proposing a new HLLC-Turkel scheme. An extension of this HLLC-Turkel method to a six-equation two-phase flow numerical model has been already presented by the author in [33], and in principle the same approach could be used readily for other HLLC-type schemes for multifluid and multiphase compressible flow models, such as the models in [13, 39]. We plan to explore other potential benefits of our reformulation of the HLLC solver. For example, we are interested in investigating possible applications to the HLLC method of the f-wave approach [2, 26] for well balancing of source terms, a technique that requires the specification of a set of average eigenvectors associated to the Jacobian matrix of the model system.

Appendix A. Roe eigenstructure for the Euler equations.

We recall the eigenstructure of the Roe matrix $\hat{A}(q_\ell, q_r)$ for a plane-wave Riemann problem in the x direction with data q_ℓ, q_r for the Euler equations. We first introduce the averages:

$$\hat{u} = \frac{u_\ell\sqrt{\rho_\ell} + u_r\sqrt{\rho_r}}{\sqrt{\rho_\ell} + \sqrt{\rho_r}}, \quad \hat{v} = \frac{v_\ell\sqrt{\rho_\ell} + v_r\sqrt{\rho_r}}{\sqrt{\rho_\ell} + \sqrt{\rho_r}}, \quad \hat{\rho} = \sqrt{\rho_\ell\rho_r}, \tag{43a}$$

$$\hat{H} = \frac{H_\ell\sqrt{\rho_\ell} + H_r\sqrt{\rho_r}}{\sqrt{\rho_\ell} + \sqrt{\rho_r}}, \quad \hat{c} = \sqrt{\kappa(\hat{H} - \hat{\mathcal{K}}) + \chi}, \quad \hat{\mathcal{K}} = \frac{\hat{u}^2 + \hat{v}^2}{2}. \tag{43b}$$

The Roe eigenvalues are:

$$\hat{\lambda}_1 = \hat{u} - \hat{c}, \quad \hat{\lambda}_2 = \hat{\lambda}_3 = \hat{u}, \quad \hat{\lambda}_4 = \hat{u} + \hat{c}. \tag{44}$$

The matrix $\hat{R} = [\hat{r}_1, \ldots, \hat{r}_4]$ of the corresponding Roe right eigenvectors is

$$\hat{R} = \begin{pmatrix} 1 & 1 & 0 & 1 \\ \hat{u} - \hat{c} & \hat{u} & 0 & \hat{u} + \hat{c} \\ \hat{v} & \hat{v} & 1 & \hat{v} \\ \hat{H} - \hat{u}\hat{c} & \hat{\mathcal{K}} - \frac{\chi}{\kappa} & \hat{v} & \hat{H} + \hat{u}\hat{c} \end{pmatrix}. \tag{45}$$

The coefficients $\hat{\zeta}_l$, $l = 1, \ldots 4$, of the Roe eigen-decomposition $q_r - q_\ell = \sum_{l=1}^4 \hat{\zeta}_l \hat{r}_l$, are:

$$\hat{\zeta}_1 = \frac{1}{2\hat{c}}\left(\frac{\Delta p}{\hat{c}} - \hat{\rho}\,\Delta u\right), \quad \hat{\zeta}_2 = \Delta\rho - \frac{\Delta p}{\hat{c}^2}, \quad \hat{\zeta}_3 = \hat{\rho}\Delta v, \quad \hat{\zeta}_4 = \frac{1}{2\hat{c}}\left(\frac{\Delta p}{\hat{c}} + \hat{\rho}\,\Delta u\right), \tag{46}$$

where $\Delta(\cdot) \equiv (\cdot)_r - (\cdot)_\ell$.

Appendix B. Roe's and HLLC semi-discrete equations for the Euler system.

We use here the grid notation introduced in subsection 4.1. We write the Roe and HLLC solution structure for a Riemann problem between the reference cell J and its neighbor K in a common framework. We denote with $\mathcal{W}_{JK}^{J,K}$ and $s_{JK}^{J,K}$ the wave and speeds corresponding to the acoustic fields, and with $\mathcal{W}_{JK}^\star$, $s_{JK}^\star$ the total middle wave (contact wave associated to the entropy wave and shear wave) and the corresponding speed, respectively. These waves and speeds satisfy $\mathcal{W}_{JK}^J + \mathcal{W}_{JK}^\star + \mathcal{W}_{JK}^K = \Delta_{JK} q$ and $s_{JK}^J \mathcal{W}_{JK}^J + s_{JK}^\star \mathcal{W}_{JK}^\star + s_{JK}^K \mathcal{W}_{JK}^K = \Delta_{JK} f(q)$. We have:

$$s_{JK}^{J,K} = U_{JK}^{J,K} \mp c_{JK}^{J,K}, \quad s_{JK}^\star = U_{JK}^\star, \quad \mathcal{W}_{JK}^{J,K} = \zeta_{JK}^{J,K} r_{JK}^{J,K}, \tag{47a}$$

$$\zeta_{JK}^{J,K} = \frac{1}{2\tilde{c}_{JK}^{J,K}}\left(\frac{\Delta_{JK} p}{c_{JK}^{J,K}} \mp \rho_{JK}^{J,K} \Delta_{JK} U\right), \tag{47b}$$

$$r_{JK}^{J,K} = \begin{pmatrix} 1 \\ \vec{u}_{JK}^{J,K} \mp c_{JK}^{J,K} \vec{n}_{JK} \\ H_{JK}^{J,K} \mp U_{JK}^\star c_{JK}^{J,K} \end{pmatrix}, \quad \mathcal{W}_{JK}^\star = \begin{pmatrix} \zeta_{JK}^\star \\ \zeta_{JK}^\star \vec{u}_{JK}^\star + \zeta_{JK}^{\star s} \vec{n}_{JK}^\perp \\ \mathcal{W}_{JK}^{\star E} + \zeta_{JK}^{\star s} V_{JK}^\star \end{pmatrix} \tag{47c}$$

$$\zeta_{JK}^\star = \Delta_{JK}\rho - \frac{\Delta_{JK} p}{(c^\star)_{JK}^2} - \left(\frac{\rho}{c}\right)_{JK}^\star \Delta_{JK} U, \quad \zeta_{JK}^{\star s} = \rho_{JK}^\star \Delta_{JK} V, \tag{47d}$$

where for the Roe solver we use the Roe averages in (43) for the interface quantities $(\cdot)_{JK}$:

$$\vec{u}_{JK}^J = \vec{u}_{JK}^K = \vec{u}_{JK}^\star = \hat{\vec{u}}_{JK}, \quad c_{JK}^J = c_{JK}^K = \tilde{c}_{JK}^J = \tilde{c}_{JK}^K = c_{JK}^\star = \hat{c}_{JK}, \tag{48a}$$

$$H_{JK}^J = H_{JK}^K = \hat{H}_{JK}, \quad \rho_{JK}^J = \rho_{JK}^K = \rho_{JK}^\star = \hat{\rho}_{JK}, \quad \left(\frac{\rho}{c}\right)_{JK}^\star = 0, \tag{48b}$$

$$\mathcal{W}_{JK}^{\star E} = \zeta_{JK}^\star \left(\frac{\hat{U}_{JK}^2 + \hat{V}_{JK}^2}{2} - \frac{\chi}{\kappa}\right), \tag{48c}$$

and for the HLLC solver we use the quantities $\check{c}^{\ell,r}$, $S^\star$ and $\rho^{\star\ell,r}$ introduced in (21), (22) and (23) replacing superscript and subscripts ℓ, r with J, K and u with U:

(49a)
$$\vec{u}_{JK}^{J,K} = \vec{u}_{J,K}\,, \quad U_{JK}^\star = S_{JK}^\star\,, \quad V_{JK}^\star = \bar{V}_{JK}\,, \quad c_{JK}^{J,K} = \check{c}_{JK}^{J,K}\,, \quad \tilde{c}_{JK}^{J,K} = \frac{\rho_J \check{c}_{JK}^{J} + \rho_K \check{c}_{JK}^{K}}{2\rho_{JK}^{\star J,K}},$$

(49b)
$$H_{JK}^{J,K} = H_{J,K}\,, \quad \rho_{JK}^{J,K} = \rho_{K,J}\,\frac{\check{c}_{JK}^{K,J}}{\check{c}_{JK}^{J,K}}\,, \quad \rho_{JK}^\star = \frac{\rho_{JK}^{\star J} + \rho_{JK}^{\star K}}{2}\,, \quad \vec{u}_{JK}^\star = S_{JK}^\star \vec{n}_{JK} + \bar{V}_{JK}\vec{n}_{JK}^\perp\,,$$

(49c)
$$(c_{JK}^\star)^2 = 2\left(\frac{1}{\check{c}_{JK}^J \tilde{c}_{JK}^J} + \frac{1}{\check{c}_{JK}^K \tilde{c}_{JK}^K}\right)^{-1}, \quad \left(\frac{\rho}{c}\right)_{JK}^\star = \frac{\rho_{JK}^K}{2\tilde{c}_{JK}^K} - \frac{\rho_{JK}^J}{2\tilde{c}_{JK}^J}\,,$$

(49d)
$$\mathcal{W}_{JK}^{\star E} = \rho_{JK}^{\star J} h_J - \rho_{JK}^{\star K} h_K - \Delta_{JK} p + \zeta_{JK}^\star \left(\frac{(S^\star)_{JK}^2}{2} + \frac{1}{2}\overline{\left(\frac{V^2}{2}\right)}_{JK}\right) + \frac{\rho_{JK}^{\star J}}{2}(U_J - S_{JK}^\star)^2 - \frac{\rho_{JK}^{\star K}}{2}(U_K - S_{JK}^\star)^2.$$

We obtain the following non-dimensionalized semi-discrete equations for the Roe's scheme and for the HLLC scheme for the Euler equations, using the Riemann solution waves defined above in the two-dimensional first-order spatial discretization (3) of the wave propagation scheme (for simplicity we do not use a special notation for non-dimensional variables):

Mass equation.

(50a)
$$\delta\frac{d\rho_J}{dt} + \frac{1}{2}\sum_{K\in\nu(J)} \rho_K \vec{u}_K \cdot \vec{n}_{JK}$$

(50b)
$$+ \tfrac{1}{2}\sum_{K\in\nu(J)} |U_{JK}^\star| \left(\Delta_{JK}\rho - \tfrac{1}{(c_{JK}^\star)^2}\Delta_{JK} p\right) - \tfrac{M_*}{2}\sum_{K\in\nu(J)} |U_{JK}^\star| \left(\tfrac{\rho}{c}\right)_{JK}^\star \Delta_{JK} U$$

(50c)
$$+ \tfrac{1}{4M_*}\sum_{K\in\nu(J)} \left(\tfrac{1}{\tilde{c}_{JK}^J} + \tfrac{1}{\tilde{c}_{JK}^K}\right)\Delta_{JK} p + \tfrac{M_*}{4}\sum_{K\in\nu(J)} \left(U_{JK}^J \tfrac{\rho_{JK}^J}{\tilde{c}_{JK}^J} + U_{JK}^K \tfrac{\rho_{JK}^K}{\tilde{c}_{JK}^K}\right)\Delta_{JK} U$$

(50d)
$$+ \tfrac{1}{4}\sum_{K\in\nu(J)} \left(\left(\tfrac{U_{JK}^K}{c_{JK}^K \tilde{c}_{JK}^K} - \tfrac{U_{JK}^J}{c_{JK}^J \tilde{c}_{JK}^J}\right)\Delta_{JK} p + \left(\rho_{JK}^K \tfrac{c_{JK}^K}{\tilde{c}_{JK}^K} - \rho_{JK}^J \tfrac{c_{JK}^J}{\tilde{c}_{JK}^J}\right)\Delta_{JK} U\right) = 0.$$

Momentum equation.

(51a)
$$\delta\frac{d(\rho\vec{u})_J}{dt} + \frac{1}{2}\sum_{K\in\nu(J)} (\rho\vec{u})_K(\vec{u}_K \cdot \vec{n}_{JK}) + \frac{1}{2M_*^2}\sum_{K\in\nu(J)} p_K\,\vec{n}_{JK}$$

(51b)
$$+ \tfrac{1}{2}\sum_{K\in\nu(J)} |U_{JK}^\star| \left(\left(\Delta_{JK}\rho - \tfrac{\Delta_{JK} p}{(c^\star)_{JK}^2}\right)\vec{u}_{JK}^\star + \rho_{JK}^\star \Delta_{JK} V\,\vec{n}_{JK}^\perp\right) - \tfrac{M_*}{2}\sum_{K\in\nu(J)} |U_{JK}^\star| \left(\tfrac{\rho}{c}\right)_{JK}^\star \vec{u}_{JK}^\star \Delta_{JK} U$$

(51c)
$$+ \tfrac{1}{4M_*^2}\sum_{K\in\nu(J)} \left(\tfrac{c_{JK}^K}{\tilde{c}_{JK}^K} - \tfrac{c_{JK}^J}{\tilde{c}_{JK}^J}\right)\vec{n}_{JK}\Delta_{JK} p + \tfrac{M_*}{4}\sum_{K\in\nu(J)} \left(\tfrac{U_{JK}^J \rho_{JK}^J}{\tilde{c}_{JK}^J}\vec{u}_{JK}^J + \tfrac{U_{JK}^K \rho_{JK}^K}{\tilde{c}_{JK}^K}\vec{u}_{JK}^K\right)\Delta_{JK} U$$

(51d)
$$+ \tfrac{1}{4M_*}\sum_{K\in\nu(J)} \left(\left(\tfrac{\vec{u}_{JK}^J + U_{JK}^J \vec{n}_{JK}}{\tilde{c}_{JK}^J} + \tfrac{\vec{u}_{JK}^K + U_{JK}^K \vec{n}_{JK}}{\tilde{c}_{JK}^K}\right)\Delta_{JK} p + \left(\tfrac{\rho_{JK}^J (c_{JK}^J)^2}{\tilde{c}_{JK}^J} + \tfrac{\rho_{JK}^K (c_{JK}^K)^2}{\tilde{c}_{JK}^K}\right)\vec{n}_{JK}\Delta_{JK} U\right)$$

(51e)
$$+ \tfrac{1}{4}\sum_{K\in\nu(J)} \left(\left(\tfrac{U_{JK}^K}{c_{JK}^K \tilde{c}_{JK}^K}\vec{u}_{JK}^K - \tfrac{U_{JK}^J}{c_{JK}^J \tilde{c}_{JK}^J}\vec{u}_{JK}^J\right)\Delta_{JK} p + \left(\rho_{JK}^K \tfrac{c_{JK}^K}{\tilde{c}_{JK}^K}\vec{u}_{JK}^K - \rho_{JK}^J \tfrac{c_{JK}^J}{\tilde{c}_{JK}^J}\vec{u}_{JK}^J\right)\Delta_{JK} U\right) = 0.$$

Total energy equation.

$$\delta\frac{dE_J}{dt} + \frac{1}{2}\sum_{K\in\mathcal{V}(J)} (E_K + p_K)\,\vec{u}_K\cdot\vec{n}_{JK} \tag{52a}$$

$$+ \tfrac{1}{2}\textstyle\sum_{K\in\mathcal{V}(J)} |U^\star_{JK}|\Big(\mathcal{W}^{\star E0}_{JK} + M_*^2(\mathcal{W}^{\star E2}_{JK} + \rho^\star_{JK}V^\star_{JK}\Delta_{JK}V) + M_*^3\mathcal{W}^{\star E3}_{JK}\Big) \tag{52b}$$

$$+ \tfrac{1}{4M_*}\textstyle\sum_{K\in\mathcal{V}(J)}\left(\frac{H^J_{JK}}{\tilde{c}^J_{JK}} + \frac{H^K_{JK}}{\tilde{c}^K_{JK}}\right)\Delta_{JK}p + \frac{M_*}{4}\sum_{K\in\mathcal{V}(J)}\left(\left(\frac{U^J_{JK}\rho^J_{JK}H^J_{JK}}{\tilde{c}^J_{JK}} + \frac{U^K_{JK}\rho^K_{JK}H^K_{JK}}{\tilde{c}^K_{JK}}\right)\Delta_{JK}U\right. \tag{52c}$$

$$\left. + \left(\frac{U^J_{JK}}{\tilde{c}^J_{JK}} + \frac{U^K_{JK}}{\tilde{c}^K_{JK}}\right)U^\star_{JK}\Delta_{JK}p + \left(\frac{\rho^J_{JK}(c^J_{JK})^2}{\tilde{c}^J_{JK}} + \frac{\rho^K_{JK}(c^K_{JK})^2}{\tilde{c}^K_{JK}}\right)U^\star_{JK}\Delta_{JK}U\right) \tag{52d}$$

$$+ \frac{M_*^2}{4}\sum_{K\in\mathcal{V}(J)}\left(\left(\left(\frac{c^K_{JK}}{\tilde{c}^K_{JK}} - \frac{c^J_{JK}}{\tilde{c}^J_{JK}}\right)U^\star_{JK} + \left(\frac{U^K_{JK}H^K_{JK}}{c^K_{JK}\tilde{c}^K_{JK}} - \frac{U^J_{JK}H^J_{JK}}{c^J_{JK}\tilde{c}^J_{JK}}\right)\right)\Delta_{JK}p\right. \tag{52e}$$

$$\left. + \left(\rho^K_{JK}\frac{c^K_{JK}H^K_{JK}}{\tilde{c}^K_{JK}} - \rho^J_{JK}\frac{c^J_{JK}H^J_{JK}}{\tilde{c}^J_{JK}}\right)\Delta_{JK}U\right) = 0. \tag{52f}$$

Above the quantity $\mathcal{W}^{\star E}_{JK} = \mathcal{W}^{\star E0}_{JK} + M_*^2\mathcal{W}^{\star E2}_{JK} + M_*^3\mathcal{W}^{\star E3}_{JK}$ is the non-dimensional quantity corresponding to the quantity in (48c) and (49d) ($\mathcal{W}^{\star E3}_{JK} = 0$ for the Roe solver and it is related to the term with $(\rho/c)^\star_{JK}$ for the HLLC solver, the term $\mathcal{W}^{\star E0}_{JK}$ corresponds to $\zeta^\star_{JK}\chi/\kappa$ for the Roe solver and to $\rho^{\star J}_{JK}h_J - \rho^{\star K}_{JK}h_K - \Delta_{JK}p$ for the HLLC solver). When preconditioning is applied, the preconditioned acoustic waves and speeds that replace $\mathcal{W}^{J,K}_{JK}$ and $s^{J,K}_{JK}$ given in (47) have the form

$$s^{J,K\,P}_{JK} = U^{J,K\,P}_{JK} \mp c^{J,K\,P}_{JK}, \quad \mathcal{W}^{J,K\,P}_{JK} = \zeta^{J,K\,P}_{JK}\, r^{J,K\,P}_{JK}, \tag{53a}$$

$$U^{J,K\,P}_{JK} = \frac{1}{2}(1+\beta^2_{JK})U^{J,K}_{JK}, \quad c^{J,K\,P}_{JK} = \frac{1}{2}\sqrt{X^{J,K}_{\beta,JK}}, \tag{53b}$$

$$X^{J,K}_{\beta,JK} = ((1-\beta^2_{JK})U^{J,K}_{JK})^2 + (2\beta_{JK}c^{J,K}_{JK})^2, \tag{53c}$$

$$\zeta^{J,K\,P}_{JK} = \frac{1}{2\tilde{c}^{J,K\,P}_{JK}}\left(\frac{\Delta_{JK}p}{\acute{c}^{J,K\,P}_{JK}} \mp \rho^{J,K}_{JK}\Delta_{JK}U\right), \tag{53d}$$

$$r^{J,K\,P}_{JK} = [1,\ \vec{u}^{J,K}_{JK} \mp \acute{c}^{J,K\,P}_{JK}\vec{n}_{JK},\ H^{J,K}_{JK} \mp U^\star_{JK}\acute{c}^{J,K\,P}_{JK}]^{\mathrm{T}}, \tag{53e}$$

$$\acute{c}^{J,K\,P}_{JK} = \mp(s^{J,K\,P}_{JK} - U^{J,K}_{JK}\beta^2_{JK}) = c^{J,K\,P}_{JK} \mp \frac{1}{2}(1-\beta^2_{JK})U^{J,K}_{JK}, \tag{53f}$$

where for the Roe solver and the HLLC solver we have, respectively,

$$\tilde{c}^{J,K\,P}_{JK} = c^{J,K\,P}_{JK}, \quad \text{and} \quad \tilde{c}^{J,K\,P}_{JK} = \frac{\rho_J c^{JP}_{JK} + \rho_K c^{KP}_{JK}}{2\rho^{\star J,K}_{JK}}. \tag{54}$$

Note that in writing the non-dimensionalized discrete equations the parameter β, which is of order M_*, is also rescaled as $\beta = M_*\tilde{\beta}$, as in [19].

REFERENCES

[1] M. R. Baer and J. W. Nunziato, *A two-phase mixture theory for the deflagration-to-detonation transition (DDT) in reactive granular materials*, Intl. J. Multiphase Flows, 12 (1986), pp. 861–889.

[2] D. Bale, R. J. LeVeque, S. Mitran, and J. A. Rossmanith, *A wave-propagation method for conservation laws and balance laws with spatially varying flux functions*, SIAM J. Sci. Comput., 24 (2002), pp. 955–978.

[3] P. Batten, N. Clarke, C. Lambert, and D. Causon, *On the choice of wavespeeds for the HLLC Riemann solver*, SIAM J. Sci. Comput., 18 (1997), pp. 1553–1570.
[4] M. Bilanceri, F. Beux, and M. V. Salvetti, *An implicit low-diffusive HLL scheme with complete time linearization: Application to cavitating barotropic flows*, Computers and Fluids, 39 (2010), pp. 1990–2006.
[5] P. Birken and A. Meister, *On low Mach number preconditioning of finite volume schemes*, Proc. Appl. Math. Mech., 5 (2005), pp. 759–760.
[6] F. Bouchut, *Nonlinear Stability of Finite Volume Methods for Hyperbolic Conservation Laws and Well-Balanced Schemes for Sources*, Birkhäuser-Verlag, 2004.
[7] Y. Colin, H. Deniau, and J.-F. Boussuge, *A robust low speed preconditioning formulation for viscous flow computations*, Computers and Fluids, 47 (2011), pp. 1–15.
[8] D. L. Darmofal and B. van Leer, *Local preconditioning: Manipulating mother nature to fool father time*, in Frontiers of Computational Fluid Dynamics, D. A. Caughey and M. M. Hafez, eds., World Scientific Publishing, 1998, pp. 211–239.
[9] S. F. Davis, *Simplified second-order Godunov-type methods*, SIAM J. Sci. Stat. Comput., 9 (1988), pp. 445–473.
[10] S. Dellacherie, *Analysis of Godunov type schemes applied to the compressible Euler system at low Mach number*, J. Comput. Phys., 229 (2010), pp. 978–1016.
[11] S. Dellacherie, P. Omnes, and F. Rieper, *The influence of cell geometry on the Godunov scheme applied to the linear wave equation*, J. Comput. Phys., 229 (2010), pp. 5315–5338.
[12] B. Einfeldt, C. D. Munz, P. L. Roe, and B. Sjogreen, *On Godunov type methods near low densities*, J. Comput. Phys., 92 (1991), pp. 273–295.
[13] D. Furfaro and R. Saurel, *A simple HLLC-type Riemann solver for compressible non-equilibrium two-phase flows*, Computers and Fluids, 111 (2015), pp. 159–178.
[14] S. K. Godunov, *A difference method for numerical calculation of discontinuous solutions of the equations of hydrodynamics*, Mat. Sb., 47 (1959), pp. 271–306.
[15] P. M. Gresho and S. T. Chan, *On the theory of semi-implicit projection methods for viscous incompressible flow and its implementation via a finite element method that also introduces a nearly consistent mass matrix. Part 2: Implementation*, J. Numer. Methods Fluids, 11 (1990), pp. 621–659.
[16] H. Guillard, *On the behavior of upwind schemes in the low Mach number limit. IV: P0 approximation on triangular and tetrahedral cells*, Computers and Fluids, 38 (2009), pp. 1969–1972.
[17] H. Guillard and A. Murrone, *On the behaviour of upwind schemes in the low Mach number limit: II. Godunov-type schemes*, Computers and Fluids, 338 (2004), pp. 655–675.
[18] H. Guillard and B. Nkonga, *On the behaviour of upwind schemes in the low Mach number limit: A review*, in Handbook of Numerical Methods for Hyperbolic Problems: Applied and Modern Issues, R. Abgrall and C.-W. Shu, eds., vol. 18, Elsevier, 2017, ch. 8, pp. 203–231.
[19] H. Guillard and C. Viozat, *On the behaviour of upwind schemes in the low Mach number limit*, Computers and Fluids, 28 (1999), pp. 63–86.
[20] N. Happenhofer, H. Grimm-Strele, F. Kupka, B. Löw-Baselli, and H. Muthsam, *A low Mach number solver: Enhancing applicability*, J. Comput. Phys., 236 (2013), pp. 96–118.
[21] A. Harten, P. D. Lax, and B. van Leer, *On upstream differencing and Godunov-type schemes for hyperbolic conservation laws*, SIAM Review, 25 (1983), pp. 35–61.
[22] C. Hirsch, *Numerical Computation of Internal and External Flows (Second Edition)*, Elsevier (Imprint: Butterworth-Heinemann), 2007.
[23] S. LeMartelot, B. Nkonga, and R. Saurel, *Liquid and liquid-gas flows at all speeds*, J. Comput. Phys., 255 (2013), pp. 53–82.
[24] R. J. LeVeque, *Wave propagation algorithms for multi-dimensional hyperbolic systems*, J. Comput. Phys., 131 (1997), pp. 327–353.
[25] R. J. LeVeque, *Finite Volume Methods for Hyperbolic Problems*, Cambridge University Press, 2002.
[26] R. J. LeVeque and M. Pelanti, *A class of approximate Riemann solvers and their relation to relaxation schemes*, J. Comput. Phys., 172 (2001), pp. 572–591.
[27] X.-S. Li and C.-W. Gu, *An all-speed Roe-type scheme and its asymptotic analysis of low Mach number behaviour*, J. Comput. Phys., 227 (2008), pp. 5144–5159.
[28] X.-S. Li and C.-W. Gu, *Mechanism of Roe-type schemes for all-speed flows and its application*, Computers and Fluids, 86 (2013), pp. 56–70.
[29] X.-S. Li, C.-W. Gu, and J.-Z. Xu, *Development of Roe-type scheme for all-speed flows based on preconditioning method*, Computers and Fluids, 38 (2009), pp. 810–817.
[30] R. Liska and B. Wendroff, *Comparison of several dierence schemes on 1D and 2D test problems for the Euler equations*, SIAM J. Sci. Comput., 25 (2003), pp. 995–1017.
[31] H. Luo, J. D. Baum, and R. Lohner, *Extension of Harten-Lax-van Leer scheme for flows at all speeds*, AIAA Journal, 43 (2005), pp. 1160–1166.
[32] S. Noelle, G. Bispen, K. R. Arun, M. Lukacova-Medvidova, and C.-D. Munz, *A weakly asymptotic preserving all Mach number scheme for the Euler equations of gas dynamics*, SIAM J. Sci. Comp., 36 (2014),

pp. B989–B1024.
[33] M. Pelanti, *Low Mach number preconditioning techniques for Roe-type and HLLC-type methods for a two-phase compressible flow model*, Appl. Math. Comp., 310 (2017), pp. 112–133.
[34] M. Pelanti, L. Quartapelle, and L. Vigevano, *Low dissipation entropy fix for positivity preserving Roe's scheme*, in Godunov Methods: Theory and Applications, E. F. Toro, ed., Kluwer/Plenum Academic Press, 2001.
[35] M. Pelanti and K.-M. Shyue, *A mixture-energy-consistent six-equation two-phase numerical model for fluids with interfaces, cavitation and evaporation waves*, J. Comput. Phys., 259 (2014), pp. 331–357.
[36] F. Rieper, *A low-Mach number fix for Roe's approximate Riemann solver*, J. Comput. Phys., 230 (2011), pp. 5263–5287.
[37] F. Rieper and G. Bader, *The influence of cell geometry on the accuracy of upwind schemes in the low Mach number regime*, J. Comput. Phys., 228 (2009), pp. 2918–2933.
[38] P. L. Roe, *Approximate Riemann solvers, parameter vectors, and difference schemes*, J. Comput. Phys., 43 (1981), pp. 357–372.
[39] R. Saurel, P. Boivin, and O. LeMétayer, *A general formulation for cavitating, boiling and evaporating flows*, Computers and Fluids, 128 (2016), pp. 53–64.
[40] R. Saurel, F. Petitpas, and R. A. Berry, *Simple and efficient relaxation methods for interfaces separating compressible fluids, cavitating flows and shocks in multiphase mixtures*, J. Comput. Phys., 228 (2009), pp. 1678–1712.
[41] B. J. R. Thornber and D. Drikakis, *Numerical dissipation of upwind schemes in low Mach flow*, Int. J. Numer. Meth. Fluids, 56 (2008), pp. 1535–1541.
[42] S. A. Tokareva and E. F. Toro, *HLLC-type Riemann solver for the Baer-Nunziato equations of compressible two-phase flow*, J. Comput. Phys., 229 (2010), pp. 3573–3604.
[43] E. F. Toro, *Riemann Solvers and Numerical Methods for Fluid Dynamics*, Springer-Verlag, 1997.
[44] E. F. Toro, M. Spruce, and W. Speares, *Restoration of the contact surface in the HLL Riemann solver*, Shock Waves, 4 (1994), pp. 25–34.
[45] E. Turkel, *Preconditioned methods for solving the incompressible and low speed compressible equations*, J. Comput. Phys., 72 (1987), pp. 277–298.
[46] E. Turkel, *Review of preconditioning methods for fluid dynamics*, Appl. Numer. Math., 12 (1993), pp. 257–284.
[47] B. van Leer, W. Lee, and P. Roe, *Characteristic time-stepping or local preconditioning of the Euler equations*, 1991. AIAA Paper 1991-1552.